

Review

# A Comprehensive Review of the Bidirectional Converter Topologies for the Vehicle-to-Grid System

Suresh Panchanathan <sup>1</sup>, Pradeep Vishnuram <sup>1</sup>, Narayanamoorthi Rajamanickam <sup>1</sup>, Mohit Bajaj <sup>2,3,\*</sup>,  
Vojtech Blazek <sup>4</sup>, Lukas Prokop <sup>4,\*</sup> and Stanislav Misak <sup>4</sup>

<sup>1</sup> Electric Vehicle Charging Research Centre, Department of Electrical and Electronics Engineering, SRM Institute of Science and Technology, Chennai 603203, India

<sup>2</sup> Department of Electrical Engineering, Graphic Era (Deemed to be University), Dehradun 248002, India

<sup>3</sup> Applied Science Research Center, Applied Science Private University, Amman 11931, Jordan

<sup>4</sup> ENET Centre, VSB—Technical University of Ostrava, 708 00 Ostrava, Czech Republic

\* Correspondence: thebestbajaj@gmail.com (M.B.); lukas.prokop@vsb.cz (L.P.)

**Abstract:** Over the past decade, there has been a great interest in the changeover from cars powered by gasoline to electric vehicles, both within the automotive industry and among customers. The electric vehicle–grid (V2G) technology is a noteworthy innovation that enables the battery of an electric vehicle during idling conditions or parked can function as an energy source that can store or release energy whenever required. This results in energy exchange between the grid and EV batteries. This article reviews various bidirectional converter topologies used in the V2G system. Additionally, it can reduce the cost of charging for electric utilities, thus increasing profits for EV owners. Normally electric grid and the battery of an electric vehicle can be connected through power electronic converters, especially a bidirectional converter, which allows power to flow in both directions. The majority of research work is carried out over the converters for V2G applications and concerns utilizing two conversion stages, such as the AC-DC conversion stage used for correcting the power factor and the DC-DC conversion stage for matching the terminal voltage. Furthermore, a bidirectional conversion can be made for an active power transfer between grid–vehicle (G2V) and V2G effectively. This review explores and examines several topologies of bidirectional converters which make it possible for active power flow between the grid and the vehicle and vice versa. Moreover, different types of charging and discharging systems, such as integrated/non-integrated and on/off board, etc., which have been used for electric vehicle applications, are also discussed. A comparison study is carried out based on several other factors that have been suggested. The utilization of semiconductors in power converters and non-conventional resources in charging and discharging applications are the two improving technologies for electric vehicles.

**Keywords:** electric vehicle; grid–vehicle; vehicle–grid; AC-DC converter; bidirectional converter; EV charging station



**Citation:** Panchanathan, S.; Vishnuram, P.; Rajamanickam, N.; Bajaj, M.; Blazek, V.; Prokop, L.; Misak, S. A Comprehensive Review of the Bidirectional Converter Topologies for the Vehicle-to-Grid System. *Energies* **2023**, *16*, 2503. <https://doi.org/10.3390/en16052503>

Academic Editors: Martina Kajanova, Marek Höger, Peter Bracinek, Pavol Špánik and Muhammad Aziz

Received: 19 January 2023

Revised: 1 March 2023

Accepted: 4 March 2023

Published: 6 March 2023



**Copyright:** © 2023 by the authors. Licensee MDPI, Basel, Switzerland. This article is an open access article distributed under the terms and conditions of the Creative Commons Attribution (CC BY) license (<https://creativecommons.org/licenses/by/4.0/>).

## 1. Introduction

An increase in demand for petroleum production, oil prices, and weather change paves an alternate solution for hydrocarbon-based transportation. Hence, developing a safe, clean, zero-emission, and high-efficiency transportation system attracts researchers' attention [1]. Moreover, 16 percent of human carbon dioxide emissions are due to the use of fossil fuels for vehicle transportation [2]. The air quality is degraded due to these emissions, creating human health issues. Hence, it is necessary to use an electric vehicle (EV) based transportation over internal combustion engine (ICE) vehicles to reduce harmful gases. When compared based on efficiency, EV gives higher efficiency than any IC engine because of the induction motor, which can be operated in braking mode so that energy can be stored back in the vehicle's battery [3,4]. The growth of plug-in hybrid electric vehicles (PHEV) is

illustrated in Figure 1. Figure 2 depicts a fair comparison with the article published in the Scopus database. After conducting a bibliometric analysis with the keywords “V2G/G2V”, “EV”, and “bidirectional converter”, it was found that 26,336, 113,007, and 10,071 articles had been published related to these topics for the past 12 years.

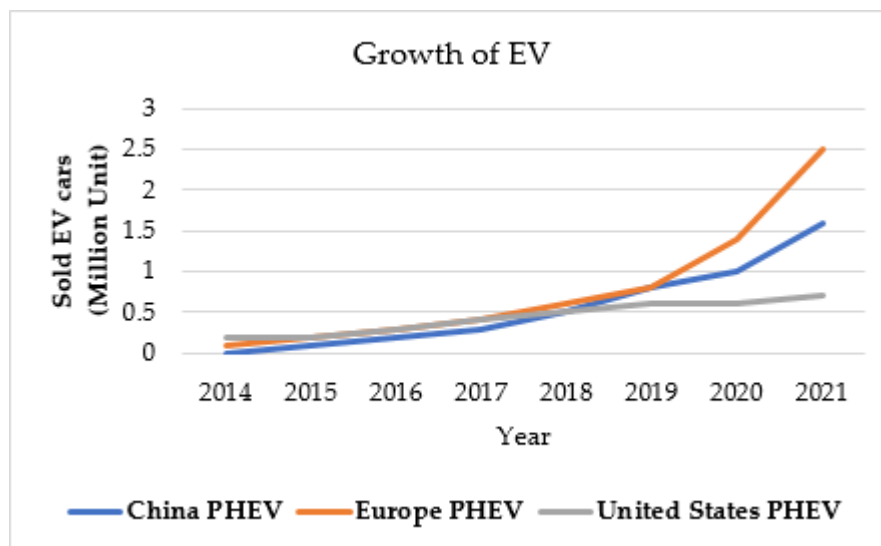


**Figure 1.** Growth of PHEV in different countries (<https://www.iea.org/data-and-statistics/charts/global-electric-car-stock-2010-2021#>) (accessed on: 14 February 2023).

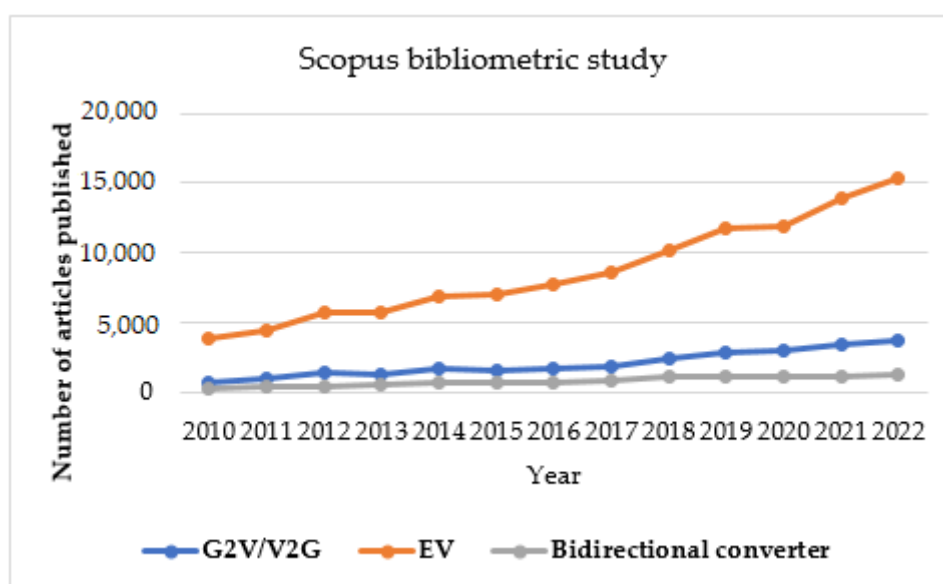


**Figure 2.** Various articles published in Scopus database with respect to the present study.

Thanks to EVs’ advantages, it is planned to replace ICE with EVs in the next few years [5]. High cost, less life span of the battery, charging system, long journey, battery management system, the introduction of harmonics to the line, low input power factor, and line losses preclude the growth of EVs in real time [6]. The success of EVs depends on developing a fast charging station with lesser power quality issues and improved power factor. Moreover, charging more vehicles at a time may result in line voltage deviation problems, frequency issues, and an increase in total harmonic distortion (THD) level in the line current during peak load conditions [7,8]. This issue can be addressed by enhancing the power system or introducing renewable energy sources (RES), such as solar, wind, etc. However, RES-based sources are intermittent and rely on the grid source and battery.

Photovoltaic panels can be directly connected to the DC-bus system to function as DC sources. The following are some of the advantages that are associated with using a DC-bus system as opposed to the more conventional AC configuration:

- When the system incorporates DC sources such as PVs, DC loads such as EVs, and energy storage devices, the system experiences lower energy conversion losses.
- A decrease in both the price and the quantity of power electronics equipment.
- There is no requirement to think about synchronizing with the utility grid or managing reactive electricity.

Since DC charge stations are faster and have more capabilities when fed from PV for charging hubs, the avoidance of conversions can increase the efficiency by around 10–15%; thus, DC fast charging can be an alternative.

Normally V2G network acts as the interface between the AC grid and the battery by allowing the bidirectional power flow between them. This bidirectional power flow should maintain the potential stability between the battery and grid with minimum current harmonics and power quality issues. As a result, power electronics converters are essential for converting AC-DC and DC-AC with minimal space requirements and maximum efficiency [9,10]. The converter's topology can be either unidirectional or bidirectional. A unidirectional topology uses more components, which are expensive, and does not make effective use of them [11]. Hence, bidirectional topologies are generally preferred for V2G-based EV systems [12]. Generally, an on-board charger includes battery storage, which results in massive weight, occupies more weight, and has space for fewer power specifications [13,14]. Whereas offline chargers do not have such an issue, it has been installed in various public locations, such as shopping malls, hospitals, educational institutions, etc. Moreover, chargers are classified as levels I, II, and III on the charging rate. Levels I and II are medium-fast chargers connected to a single-phase AC power supply, and only Level III is the off-board fast charger, which uses a three-phase AC supply as the source [15–17].

The EV-based system provides more flexibility than ICE because of the different propulsion systems, battery storage systems, electric motors, and charging units. EVs' power demand is met by the different converter topologies and energy management systems [18]. Various research has been carried out to construct a novel technical solution to improve the EV system's performance. However, there is a need for a comprehensive review for the kindle researcher to conduct their research in EV. Hence, this article proposes a comprehensive review of EV systems, which includes power electronic converters, battery-to-grid and grid-to-battery, and charging/discharging systems.

The organization of the paper is carried out as follows. Section 2 includes a bidirectional converter for EV application. Conductive and inductive chargers, dischargers, and their comparison are explained in Section 3 and Section 4, respectively. Energy management in EV and the recent trends are described in Section 5 and Section 6, respectively. The main theme of the paper is summarized in Section 7. The overall conclusion of the article is enumerated in Section 8.

## 2. Power Converters for EV Applications

Innovation in power electronics has extensively contributed to the growth of EV technology. The heart of the EV system is the electric motor and battery management system. Depending on how the power flows, converters used to charge batteries are either one-way or two-way. Quite often, bidirectional converters are preferred for practical application because the system has less weight, volume, and cost and better component utilization. Hence various bidirectional topologies used for battery charging are reviewed in this section.

### 2.1. Semiconductor Device Level

The performance of the power electronics-aided system relies upon the growth of wide band gap semiconductor switches. The material of the semiconductor switches include silicon carbide (SiC)- and gallium nitride-based devices, has high breakdown voltage, band gap, saturation velocity, and thermal conductivity. This results in devices with higher power handling capacity, small size, and lesser losses with a unidirectional and bi-directional conducting nature. Moreover, the switches can be operated in high switching frequencies with high power density and high voltage handling capacity.

At the beginning of the 19th century, SiC-based devices were generally preferred for high voltage, switching frequency, and temperature applications [19]. They are recently available in the market with 1.7 kV and 13 mΩ on-state resistance. Moreover, 3.3 kV, 6.5 kV, and 10 kV devices are narrowly available due to the problem in market challenges [20]. GaN devices are used for low-power applications (<600 V) and provide excellent switching and conductance performance [21].

### 2.2. Full-Bridge Bidirectional Converter and Reversible DC-DC Converter

This architecture of any full bridge (FB) is the most prevalent type of bidirectional AC-DC converter (BADC) topology because of the versatility of its circuit construction. The IGBT-based on BADC was described by Pinto et al. [14], and it was integrated with a non-isolated DC-DC converter using a bus capacitor. Along with G2V and V2G, this converter makes it possible to operate in a third mode known as vehicle-home (V2H). In this mode, the electric vehicle battery source can be utilized as a voltage-controlled source for supplying the domestic load when the main power supply is interrupted. The BADC functions as an active rectifier when it is set to the G2V mode. When operating in the V2G mode, BADC operates as a regulated source of current that contributes electricity to the utility grid for maintaining the power factor. Figure 3 illustrates the structure of a full-bridge (FB) bidirectional converter and a reversible DC-DC converter.

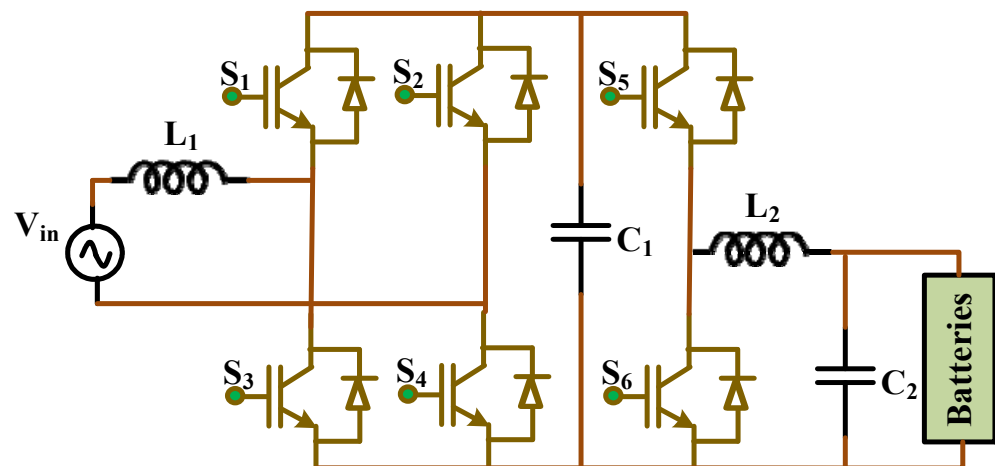


**Figure 3.** Full-bridge bidirectional converter and reversible DC-DC converter.

#### 2.2.1. Eight-Switch Topology

In [18], a non-isolated half bridge bidirectional DC-DC converter coupled DC link is proposed and depicted in Figure 4, where an induction motor is connected at the load end for propulsion application. This combined form of converter acts as an inverter during motoring mode and the action of the rectifier under regenerative braking mode. For the different operating modes, such as V2G mode and G2V mode, the THD level of the input side is drastically reduced by incorporating an improved proportional resonant controller (PRC). Moreover, an indirect scheme of field-oriented control (FOC) based on particle swarm optimization (PSO) is introduced to reduce the loss and increase efficiency. This

system predominantly improves reliability by reducing the heating effect of current ripple and THD.

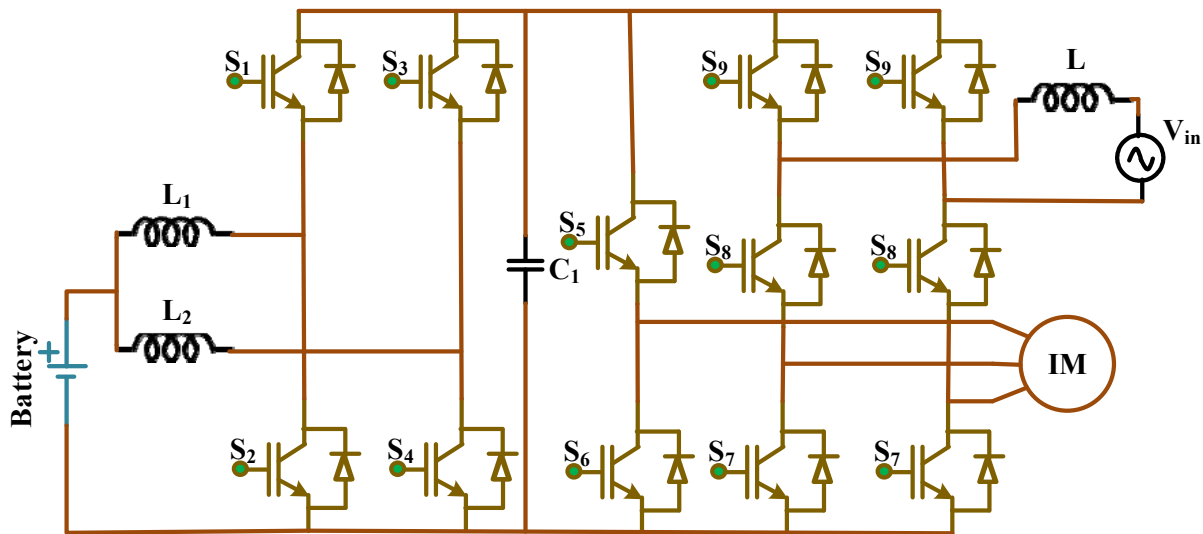


Figure 4. Non-isolated half bridge bidirectional DC-DC converter.

### 2.2.2. Three-Level Topology

The suggested topology aims to shape the grid current waveform by ensuring that switching between voltages with variable pulse width happens appropriately. In [19], reported in the V2G system, the structure comprises two diodes and six-number switches with a non-isolated BDC. However, the system depicted in Figure 5 has a BADC linked with BDC with five switches and diodes [20]. Capacitors  $C_1$  and  $C_2$  isolate both converters, and for generating the required gate pulse for all the IGBTs, a feedback controller is added with a low pass filter. Apart from V2G and G2V, the proposed technique aids regenerative braking, which delivers extra power to plug-in hybrid electric vehicles during acceleration. This bidirectional converter produces reduced current harmonic and noise. The voltage stress felt by all the components is less, and a smaller input side inductor limits the cost and size, even though the applications of BADC suffer from more conduction loss.

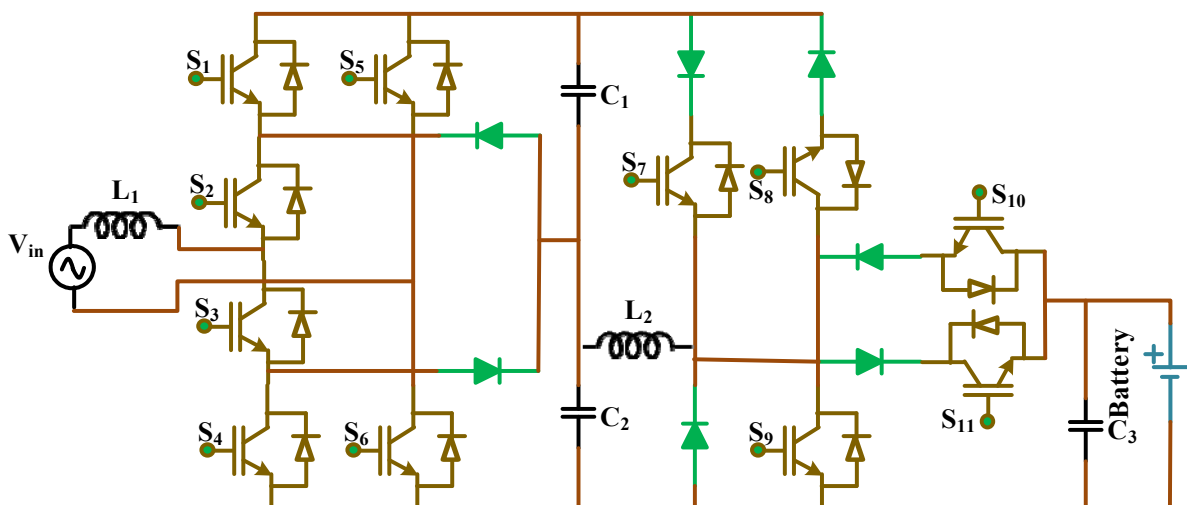


Figure 5. Five switches non-isolated buck-boost BDC.

The complete bridge BADC structure combined with an asymmetrical three-level structure significantly reduces switching loss and inductor size, as shown in Figure 6 [21].

Four switches create the proposed structure,  $S_1$  to  $S_4$  and an asymmetrical three-level converter with the switches  $S_5$  to  $S_8$ . From the structure, it is clear that a path made between the converter and the battery to be charged reduces the rating and power loss of BDC. Thus, the system can produce an efficiency of not less than 97% in both modes of operation when choosing a wide range of voltage.

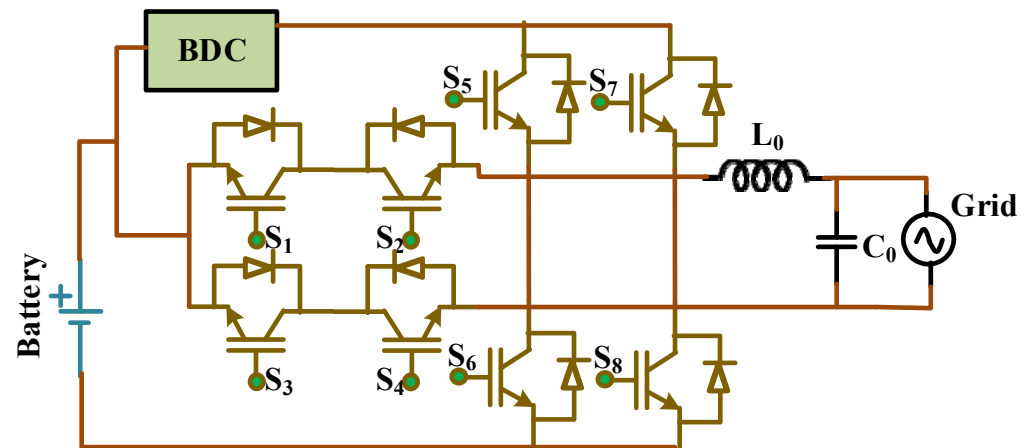


Figure 6. Asymmetrical three-level converter.

### 2.2.3. Single-Stage Topology

In [22], the author proposed a single-stage topology of BADC incorporated with a power factor correction (PFC) converter comprising half-bridge and FB topologies on both the input and output sides. This topology achieves zero-voltage switching (ZVS) on the input side by properly combining frequency and phase shift modulation. Moreover, the input side rectification is removed with the help of switches that are connected in the opposing direction of the input, as depicted in Figure 7. Here,  $L_m$  and  $L_2$  represent magnetizing inductance and transformer leakage inductance, respectively. Grid side filtering component consisting of  $L_1$ ,  $C_1$ , and  $C_2$  avoid the injection of harmonic content towards the grid and maintains a unity power factor during power flow vehicle to grid. During the positive half-cycle rectification, switches  $S_1$  and  $S_3$  are switched ON at high-frequency levels, and  $S_2$  and  $S_4$  are at low-frequency levels.

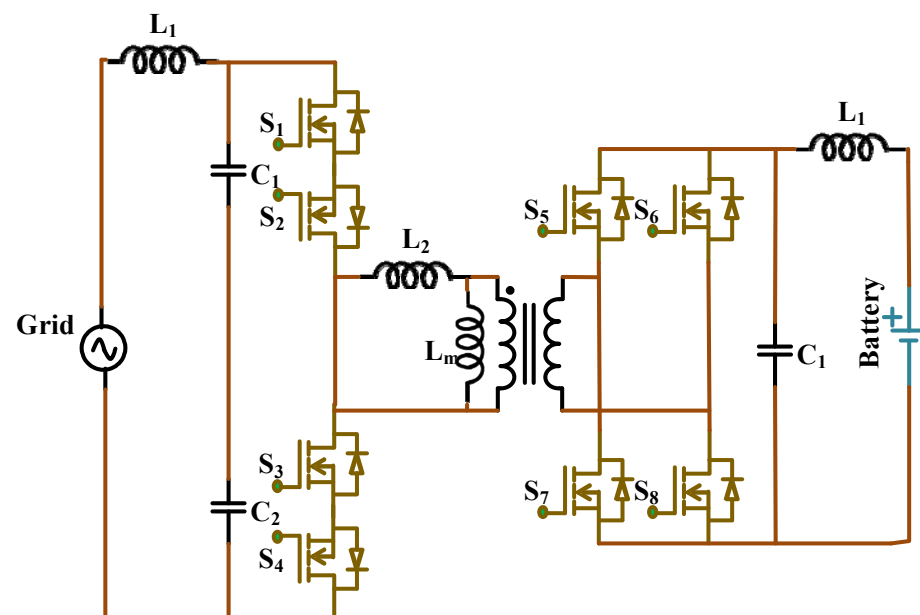


Figure 7. Single-stage isolated BADC.

Similarly, under adverse half-cycle conditions, switches  $S_2$  and  $S_4$  are switched ON at high-frequency levels, and switches  $S_1$  and  $S_3$  are switched ON at low-frequency levels. In this topology, variable dependent load frequency is maintained with the frequency ranges from 20 kHz to 120 kHz, but the frequency level is maintained less during low load conditions. This makes the design complication of the controller. The proposed topology in [22] reveals a similar type of converter. However, the half-bridge topology is replaced by the full-bridge topology on the input side, leading to increased power devices. The inductive capacitor tank circuit provides the soft switching of the power device circuits to obtain a higher efficiency value [23].

In the paper [24], the author suggested a center-tapped structure with a cyclo-converter-based topology on the grid side and a FB topology on the battery side, as shown in Figure 8. This topology is made up of four power switches ( $S_1$ – $S_8$ ). Two switches are fully active, and the other creates paths for freewheeling. Center-tapped transformers are used to isolate from the power circuit, and leakage inductance and parasitic capacitances are used for soft switching operation. During V2G mode, the components on the battery side are connected with pulse width modulation (PWM). In contrast, the other devices connected at the grid frequency are swapped so that battery-side devices can achieve ZVS.

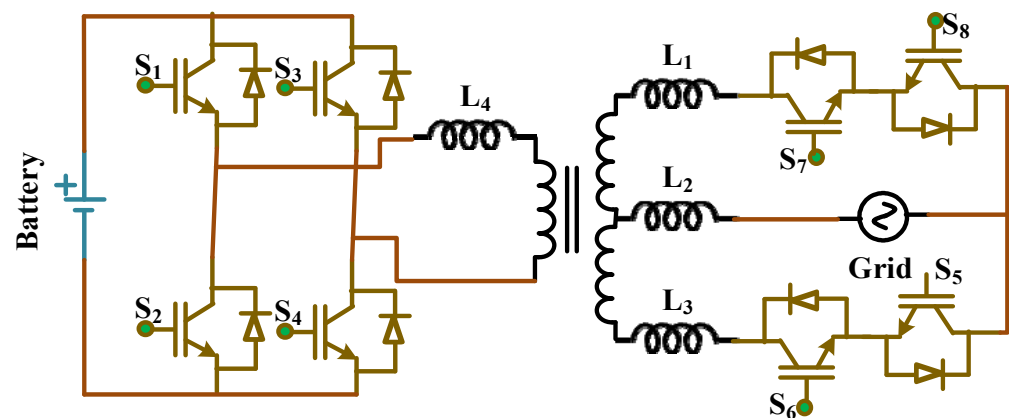


Figure 8. Cyclo-converter-based full bridge topology.

On the other hand, in grid-to-vehicle mode, the devices in the battery-side converter are modulated so that the sinusoidal pulse width modulation SPWM at grid frequency is generated. The soft switching characteristics increase the power density at reduced switching frequencies. However, an accurate design is carried out for the transformer to match the leakage currents on the secondary side.

#### 2.2.4. Topology Based on Matrix Converter

Typically for power frequency to AC grid voltage conversion into high-frequency ac grid voltage, it requires the AC voltage to DC voltage and DC to AC conversion stages, and also more expensive capacitors. However, these heavy and costly components are eliminated by matrix converters, which is a direct type of AC-to-AC converters presented by the author in [25]. Here, a matrix converter for a three-phase system has been suggested for the V2G system, which utilizes an optimized sectional topology for reducing the current ripples during the charging period [25]. It is proposed to use bidirectional, series-connected, antiparallel IGBTs with freewheeling diodes that are connected to a CE structure. In this arrangement, six switches of bidirectional type and LC filters are connected both at the grid converter side and battery side converter, as shown in Figure 9.

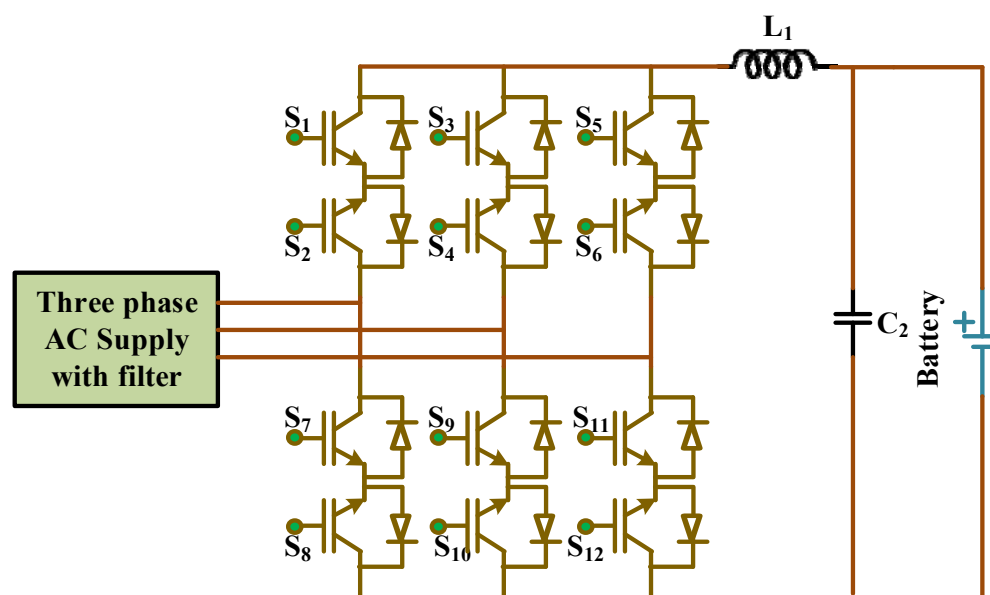


Figure 9. Non-isolated matrix converter.

The main reason for connecting on the grid-side converter is that the LC filter prevents high-frequency injections from the grid. Similarly, the LC filter connected at the battery side prevents high-frequency ripples. To improve the synchronization of V2G voltage on the grid side, digital PLL is incorporated, and two PI controllers maintain constant current and voltage profiles.

On the other hand, it is required to add a controller in the G2V mode to stabilize the operation by reducing the damping. The controller used in the proposed system has merits such as more efficiency, reliability, quick response over the transients, and, importantly, flexibility in the power factor correction. Even though it has some advantages, it also experiences some demerits during the active power flow from vehicle to grid and vice versa. Additionally, the life of the battery can be reduced due to reduced ripples in the current.

In [26–28], the author proposed some topologies-based matrix converters for V2G systems. The converter shown in Figure 10 gives an isolated bidirectional converter where a square wave-modulated converter is coupled with a resonant matrix converter through a high-frequency transformer. This topology consists of a resonant inductor and capacitor  $L_1$  and  $C_1$ , respectively. A unipolar SPWM controller is incorporated for synchronized operation with the grid. The grid side voltage can be adjusted with the help of the PWM rectifier voltage on the p transformer primary side. The tank circuit can ensure a lower level of VA transformer rating. Higher efficiency can be maintained by properly turning ON the power devices when ZVS is present and OFF under ZVS conditions. This type of BADC structure yields quick charging of EVs, quick response to transients on the demand side, lower THD, easy control systems, higher reliability, and power density. However, the topology faces low-frequency ripples during battery charging and uses more power components. In [27], the same isolation topology with a single-phase matrix is suggested. In [28], the EV battery–grid interfacing is performed by the proposed matrix converter where inductor–capacitor resonant dual active bridge topology was incorporated. The structure can charge and discharge more than one EV in parallel.

### 2.2.5. Recent Trends

Components such as GaN and SiC, which has a wide band gap, can enhance the functionality of substantial power converters [29,30]. From the researcher’s point of view, all the silicon-based devices can be replaced with GaN and SiC devices shortly [31] as

they can give better thermal efficiency, low value of reverse recovery charge, higher power density, high-frequency operation [31,32] and high blocking capability.

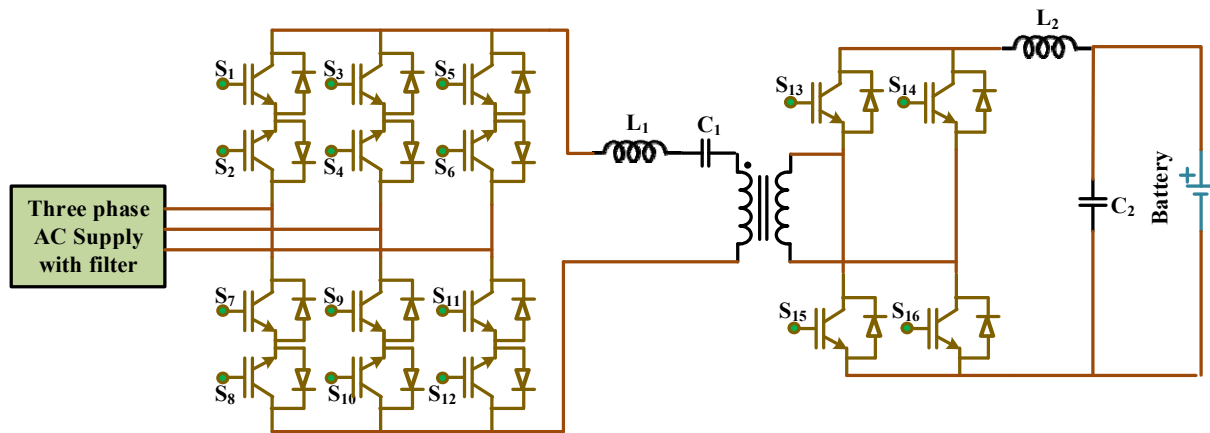


**Figure 10.** Isolated matrix converter.

### 2.3. Bidirectional DC-DC Converter

BDC is a type of DC-DC converter capable of correcting the control instruction that causes the power flow to change its direction. They allow DC voltage to be converted between two levels in both directions [33]. The magnitude of one of the two voltages is more than that of the other. The following are the two clearly defined roles that a BDC type converter plays in a vehicle-to-grid connectivity subsystem: during the mode of V2G, the voltage of the battery is altered to DC side voltage, and during G2V mode, or the charging mode, the voltage is converted to the proper level of charging voltage. A Bidirectional type DC-DC converter (BDCs) charges the EV batteries followed by two stages of charging, such as a constant current mode [15,16] and a constant voltage mode. Bidirectional-type DC-DC converters (BDCs) run at higher switching frequencies in such a way as to enhance the capacity of power density. As a result of devices being turned ON and OFF quickly, HF noise is produced, which harms other grid-connected equipment and generates electromagnetic interference (EMI) in the grid. Therefore, while designing BDCs, reliable EMI mitigation and control techniques must be adopted.

#### 2.3.1. Isolated Topologies

The voltage-fed dual active bridge (DAB) design is one of the most often used isolated types of bidirectional DC-DC converters (BDCs) for an extended range of voltage applications such as V2G [17,34]. This conventional converter has two complete bridges with four transistors each, and the HF transformers are used to isolate switches. Phase shift modulation methods are mainly used to regulate the flow of power. Galvanic isolation, the flexibility of control, the soft-switching capability of soft-switching, less voltage stress, higher efficiency, high capability of power [35], density, symmetrical, and [34] expandable design are some of the key benefits of the DAB architecture. The restricted voltage conversion range, high circulating current [36], and increased injection of reactive power [37] are some of the problems associated with voltage-fed converters. The BDC uses snubber capacitors to ensure the power devices' soft-switching. The author of [38] describes a high-power BDC system that consists of a three-phase FBBADC connected to a dual active bridge BDC as illustrated in Figure 11. Switches  $S_1$  to  $S_6$  comprises the BADC, whereas  $S_7$  to  $S_{13}$  comprise the BDC. The BADC has been controlled under direct current control, while the BDC has been controlled under single-phase shift modulation.

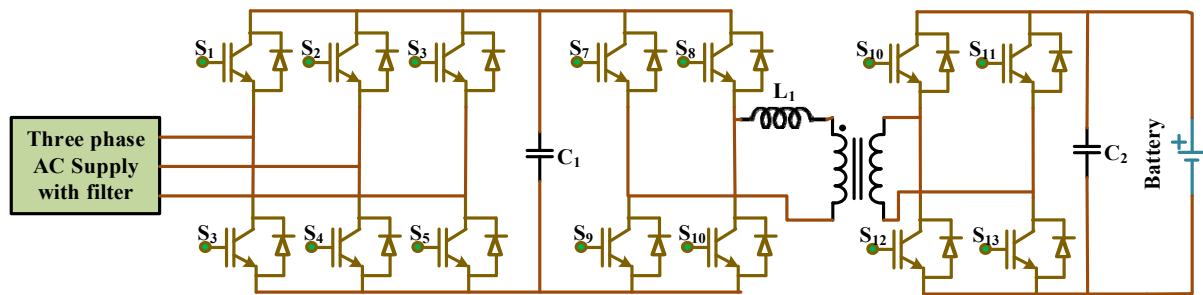


Figure 11. Three-phase BADC and BDC.

The battery can be charged using either a constant-current or constant-voltage technique. The PQ control technique incorporated in the BADC is utilized in the V2G mode to regulate the injection of reactive power and real power to the grid side. Current-fed type dual active bridge BDCs have a broad input voltage range, minimum value input current, minimal diode ringing, less ratio in transformer turns, zero loss in duty cycle, high voltage gains [39], fewer diodes, reduced transformer turns ratio, and improved current control capabilities [40,41]. However, to reduce the switching losses in current-fed converters, active clampers or snubbers must be used to reduce the spikes, which can increase the cost. In isolated phase-shifted BDCs, snubber capacitors are usually used across the switching devices [36,42]. It aids in reducing transients in switching, voltage spikes, current spikes, electromagnetic interferences, and the problem in recovery of diode reverse. In order to maximize the energy circulating and extend the range of soft-switching converters, an adequate inductor design is necessitated. The current and voltage-fed dual active bridge structure is used [35]. The current-fed bridge type is utilized for buck mode operation, and the current-fed type structure is implemented during boost mode operation. The author discussed a secondary modulation-based dynamically clamped soft-switching current-voltage fed dual active bridge BDC in [36] that switches primary devices at zero current switchings (ZCS) and secondary side components at ZVS independently. BDC consists of the transformer's leakage inductance  $L_1$ , as shown in Figure 12. The system's footprint and magnetics cost decreased by using a high switching frequency of high value of 100 kHz. This type of converter is extendable for higher-power V2G applications and can be interleaved. The main limitation is that it operates with eight active power components, which raises the BDC's conduction losses. Figure 13 depicts current-voltage supplied half-full bridge BDC. An identical modulation approach has been applied in [42]. The benefits of having six power switches rather than eight, zero voltage source for secondary devices instead of ZCS include less peak value of current through devices, less loss in conduction, and less circulating current.

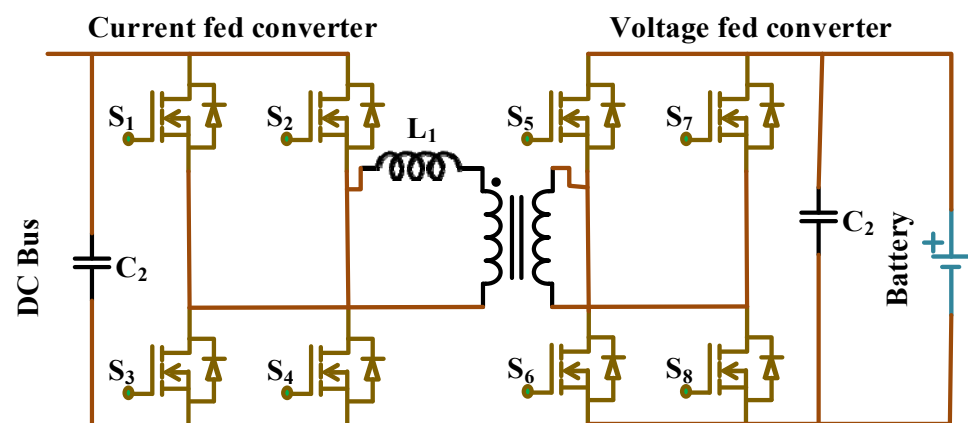


Figure 12. Current fed full bridge snubber less converter.

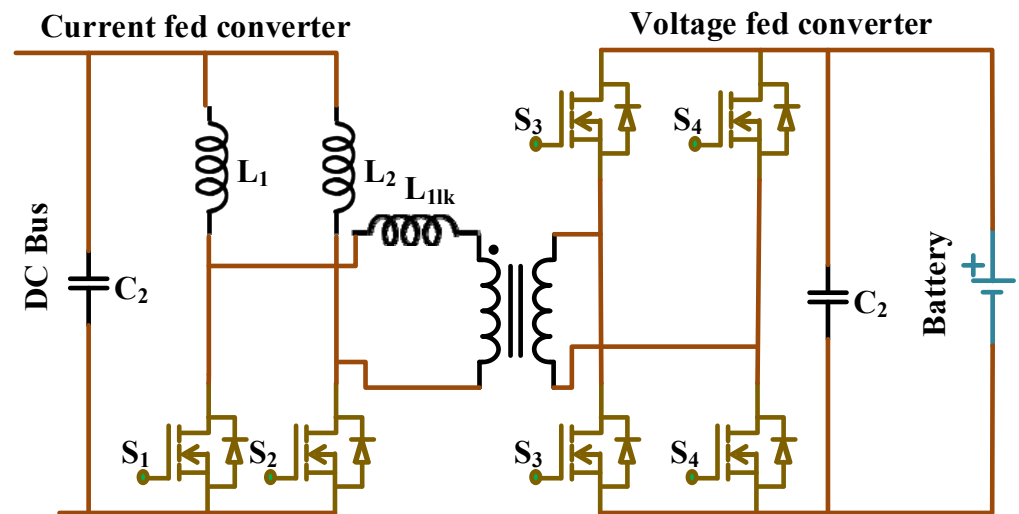


Figure 13. Current fed half bridge snubber less converter.

### 2.3.2. Non-Isolated Type Topologies

These topologies use an inductor to transfer the energy toward the load, and the controller architecture is quite simple. The inductor can store magnetic energy when the switch is ON under boost operation and release it when it is switched OFF. Because of the absence of the high-frequency isolation transformer, the benefits of non-isolated methodology are that it uses less number of switches and passive components, has lesser costs, and has a minimum footprint than isolated methodology [18]. The non-isolated configurations, however, do not adhere to the safety requirements.

Furthermore, compared to isolated configurations, non-isolated topologies have reduced voltage magnitude, range of conversion, and control flexibility [41,43–48]. The common, typical non-isolated BDC architecture is the buck–boost mode of operation, in which the functions of BDC are as a buck converter mode in the grid to the vehicle and as a boost converter mode in the vehicle to grid. The non-isolated buck–boost mode of operation employs only two switches in BDCs to accomplish the DC-DC conversion step, but a five-switch non-isolated buck–boost mode BDC architecture is presented in [20]. It was reported that a FB type of bidirectional converter linked with a non-isolated [44] buck–boost converter could regulate both real power and reactive power. The phase angle and voltage provided by the vehicle to the grid are synchronized with these grids using a PLL algorithm in  $\alpha$ - $\beta$  coordinates. Here BADC employs a d-q frame controller to regulate reactive power. The BDC uses a PI controller to regulate real power.

The electric vehicle battery is charged by a controller using constant current, voltage, and power techniques. Here the BADC utilizes inductor filters on the grid side, and the BDC utilizes LC filters on the battery side. Khan et al. developed a non-isolated cascaded buck–boost mode of BDC suggested in [43], which enables input voltage and output voltage range overlap for electric vehicles with vehicle-to-grid capabilities. The input and output voltage ranges are overlapped using four switches with an intermediate capacitor in this configuration. Figure 14 shows the circuit, where  $C_1$  stands for the intermediate DC-link capacitor. Two distinct PI controllers control the output voltage and the intermediate DC-link voltage. PWM serves to operate the BDC. With the presence of both modes, G2V and V2G, the compensation of reactive power can be performed easily and, thus, the compensation of power factor. The suggested system combines a non-isolated two-phase interleaved half-bridge BDC design with the neutral-clamped BADC [48]. Coupled inductors have been employed to minimize charging current ripple, maintaining the model simple and mode-friendly.

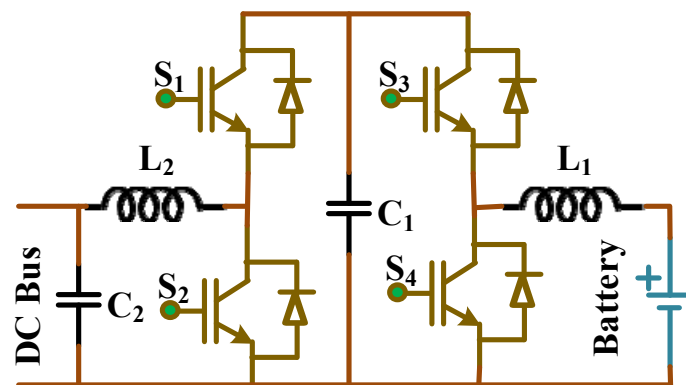


Figure 14. Non-isolated cascaded buck–boost converter.

### 2.3.3. Resonant Topologies

Researchers are substantially investigating resonant-type DC-DC converters for a large range of voltage applications. As they do not require clamp or snubber circuitry, they provide incredible works on high frequency, outstanding efficiency, minimal electromagnetic interference, and lesser components [37]. Resonant converters have better efficiency for low loads than phase-shifted DAB and similar efficiency for huge power transfers [49–57]. However, because of the low input impedance of the filter capacitors, the preponderance of resonant converters experiences a significant start-up surge current. Despite having outstanding switching characteristics, the PWM resonant converter is mostly a buck-mode type converter. It is unsuitable for BDCs and performs both buck mode and boost mode operations. Figure 15 illustrates an isolated full-bridge pulse width modulation [50] resonant type BDC. The converter comprises a series of LC resonant tanks made of  $L_f$  and  $C_f$  in the isolation transformer's primary side and a capacitor-based charge pump connected in series with the second part for resonant PWM operation, which facilitates enhanced functioning. The negative impacts of an extremely high level or low level of switching frequency are reduced by PWM control. A significant value of  $C_v$  is necessary to prevent the LC tank's resonance frequency from affecting  $C_v$ , and it causes the BDC to be large and expensive. Additionally, the bidirectional DC-to-DC converter has a sluggish overvoltage response. The author created a CLLLC-type isolated double voltage-fed full-bridge bidirectional DC-DC converter with its phase angle control and incredibly high conversion efficiency in both modes [37].

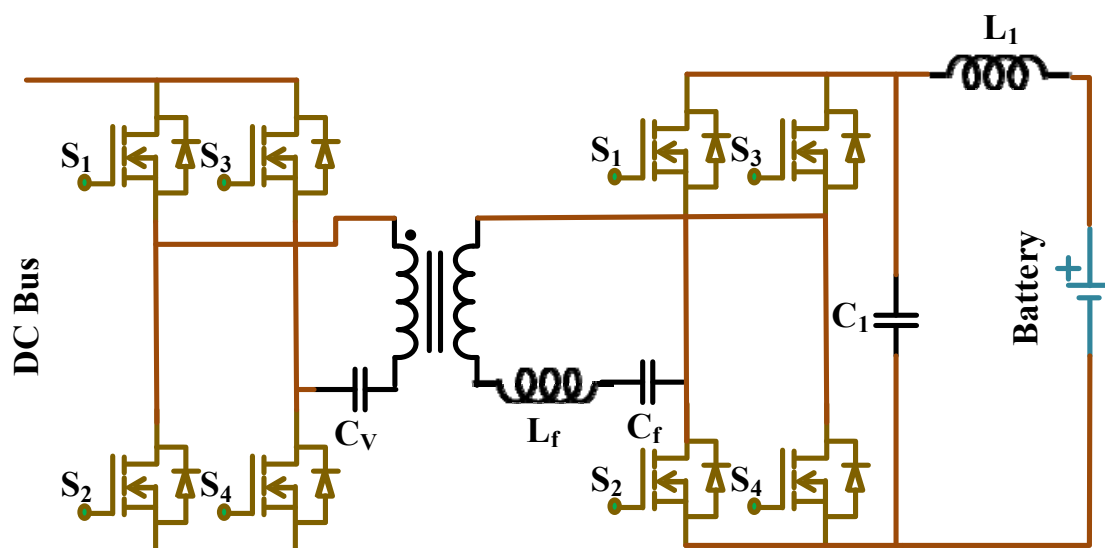


Figure 15. Isolated full-bridge type BDC.

An approach with variable switching frequency was used to ensure a zero-voltage source under different load conditions. Figure 16 shows the BDC where the CLLLC-type resonant network is comprised of capacitances at resonant conditions  $C_1$  and  $C_2$ , resonant inductors  $L_1$  and  $L_2$ , and  $L_m$  transformer magnetizing inductor. The transformer's series leakage inductance is an element of the resonant network. Switches (IGBT)  $S_1$ – $S_4$  are used in the primary side switching, whereas switches  $S_5$ – $S_8$  (MOSFET) are utilized at the secondary side power switches since MOSFETs are on the primary side, resulting in an appropriate switching loss. The secondary circuit is formed by adding the inductive element  $L_2$  and keeping the switching frequency somewhat greater when compared with the typical operating frequency, which can help solve the issues of a significant starting level surge current.

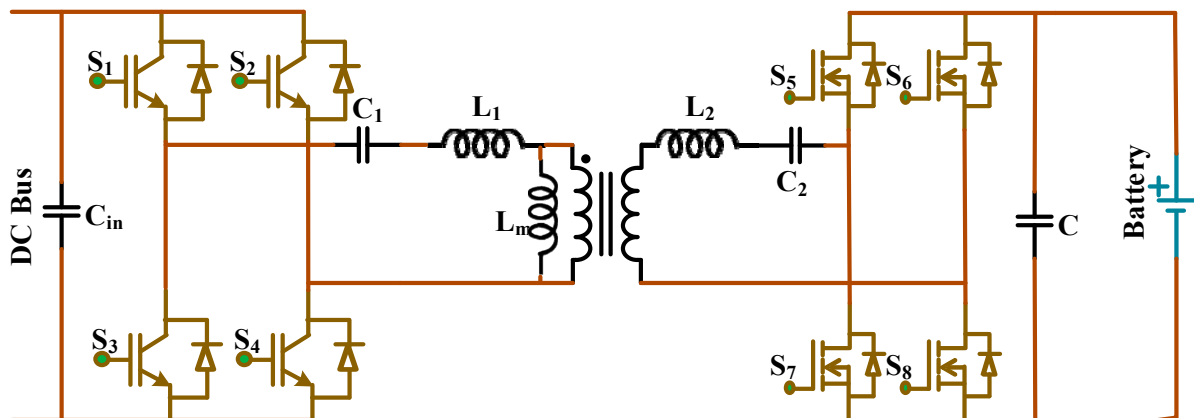


Figure 16. CLLLC-type resonant converter.

The dual resonant type of BDC was presented in [32], which connects three converter bridges type using a three-winding transformer to enable G2V and V2G operations and also from high voltage (HV) charging to low voltage (LV) charging. Reduced effect of saturation, fewer magnetizing losses, a fewer footprint, and minimum cost are the implications of converting three windings types into a single transformer whose combined topology is depicted in Figure 17. Here both the primary-side and secondary-side converters consist of a half-bridge type with capacitors  $C_1$  and  $C_2$ . However, the tertiary side is of a FB synchronous converter which also reduces the conduction loss and the circulating current. Switches on the tertiary side are silicon MOSFETs, while the primary-side and secondary-side switches are silicon carbide MOSFETs with a large drain in voltage and less turn-on resistance.

On the tertiary side, switches  $S_9$  and  $S_{10}$  comprise the back-to-back combination, which helps disconnect the LV side load whenever needed. An LLC-type converter and a CLLLC-type converter are combined in the integrated resonant converter. Here,  $L_1$  is the primary side leakage inductance;  $L_2$  is the leakage inductance on the secondary side;  $L_m$  is the magnetizing transformer inductance; and four resonant split capacitors,  $C_1$ ,  $C_2$ ,  $C_3$ , and  $C_4$ , make up the CLLLC resonant network. Together with LLC resonant,  $L_1$ ,  $L_m$ ,  $C_3$ , and  $C_4$  form a network.  $C_1$ ,  $C_2$ , and  $L_1$  form a resonant network in grid-to-vehicle mode.  $C_3$ ,  $C_4$ , and  $L_2$  make up the vehicle's resonant network to the grid and H2L modes. By employing PI controllers, an adjustable DC-link voltage control scheme ensures that the BDC maintains close to the resonant range of frequency over the full output voltage range. Because of the ZVS turning ON of components over a broad input and output range of voltage, the converter exhibits great efficiency and power density capabilities. However, a transformer with three-winding and two significant leakage inductances is required, which is costly and complex to make. For V2G systems, an isolated double semi-bridge CLLC-type resonant bidirectional type DC-DC to converter was suggested in [52].

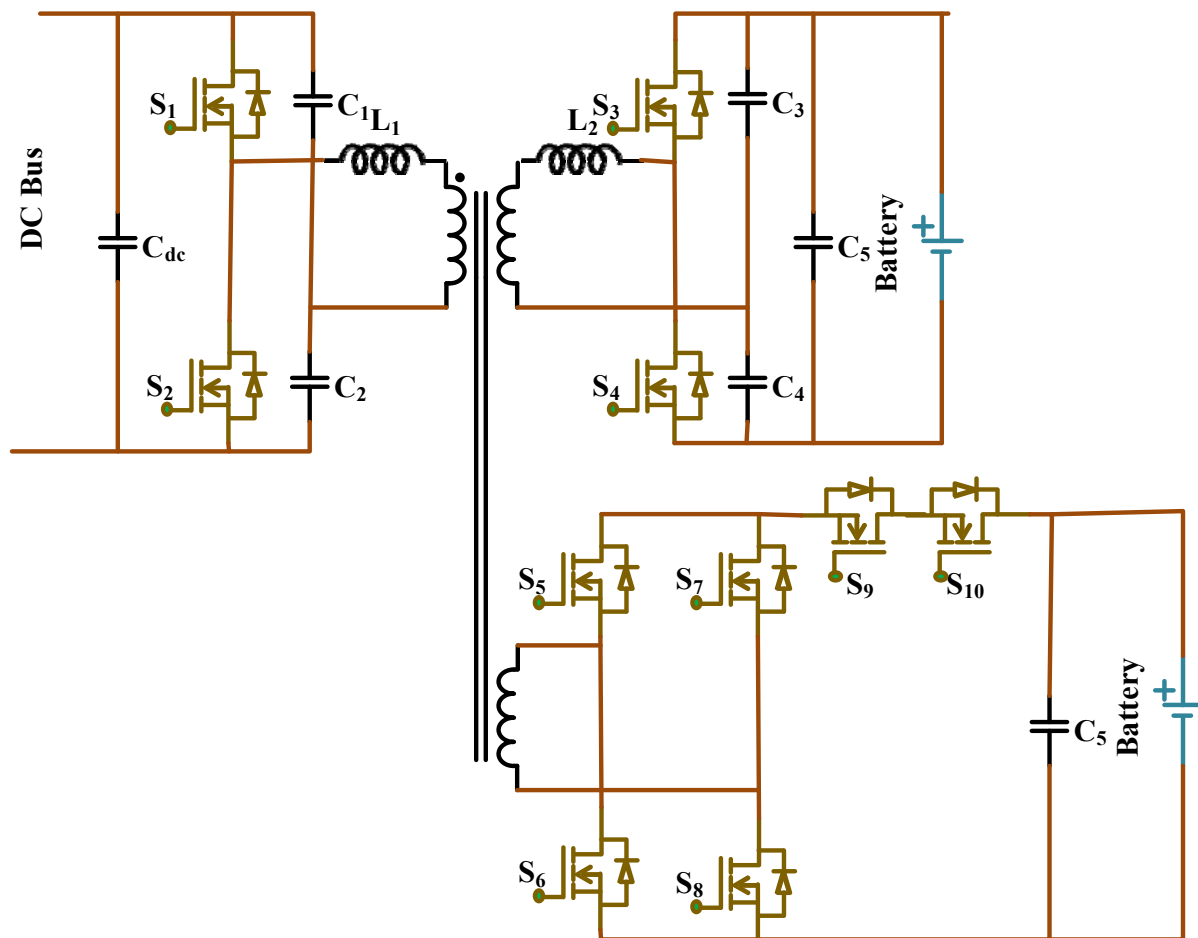
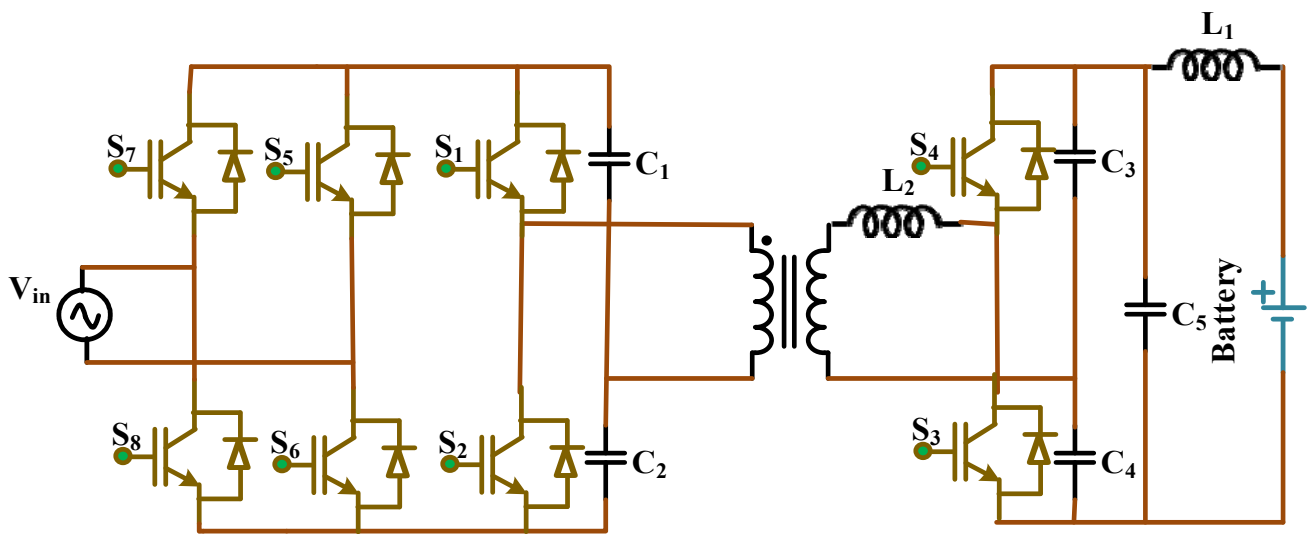


Figure 17. Dual type output resonant BDC.

The system employs the HF transformer's leakage and magnetizing inductors as resonant inductors. Resonant capacitors are replacing the half-bridge DC capacitors. A frequency at a high resonant of 130 kHz was used to reduce EMI and increase the converter's power density. In order to enhance system efficiency, the technology ensures gentle switching of the components in either operating condition while running at a broad output voltage range. The secondary resonant tank circuit reduces circulating current and related conduction loss through synchronous rectification and dead-band management. This leads to a 1.7% increase in system efficiency. When employed as a source of energy storage, electrolytic capacitors threaten a BDC in terms of power density and reliability.

The author presented a sinusoidal type charging methodology for the electric vehicle battery that was suggested in [53]; it moves away from the need for electrolytic capacitors, as shown in Figure 18. Here, FB-BADC with an LCL filter is connected to an isolated half-bridge series resonant converter with an LC filter by capacitors  $C_1$  and  $C_2$ . In transformer  $L_1$ , the leakage inductance, two resonant capacitors,  $C_3$  and  $C_4$ , work together to form the resonant network. Only HF ripples are eliminated by the LC filter and capacitors  $C_1$  and  $C_2$ , enabling low-frequency unwanted ripples for the electric vehicle battery. The BDC is controlled by PI controllers and has a predefined switching frequency. The BADC and LCL filter work together to regulate the power factor control and minimize the grid harmonic injection. The zero current source switch makes ON/switch-OFF for the whole load range, enabling the converter to operate at high efficiency. The switching devices with conduction losses constitute most system losses, even though switching losses are pretty low. However, sinusoidal charging increases the battery temperature when charging by reducing the battery capacity.



**Figure 18.** A full-bridge bidirectional DC converter with an LCL filter.

#### 2.3.4. Current Trends

Comprehensive bandgap technologies such as silicon carbide and gallium nitride are the main focus of current research because they provide substantial benefits over other silicon switch alternatives for large energy applications. According to [31], an all-SiC architecture for 10 kW isolated soft-switching devices such as semi and full-bridge LLC type resonant bidirectional DC-DC converter exhibited an efficiency boost of 0.7–2% over employing all-Si devices. Gallium nitride FET promises similar benefits, including lower input capacitance, higher dielectric strength, switching frequency, lesser Miller charge, higher operating temperature, lower reverse-recovery voltage, and smaller non-active components [30]. These advantages suggest that Gallium nitride FETs can switch to previously inaccessible or unfathomable performance areas. A GaN-based DAB and BDC that runs at 500 kHz and promises to reduce the space by 90% of the DC link capacitor via sinusoidal charging have been disclosed in [30].

#### 2.3.5. Comparison of Different Types of BDC

One of the most common types of non-isolated bidirectional DC-DC converters is the buck-and-boost type of converter. On the other hand, the most general isolated bidirectional DC-DC converter type is a full bridge type. As the isolation transformer is not present in the non-isolated methodologies, it offers advantages such as a lesser footprint, lighter weight, low amount, and easy control. Components in these converters are employed to their maximum potential using fewer switching devices. The substantial conduction loss produced by the substantial current flowing across the passive components and switching devices, however, reduces the power density capabilities of these converters and affects their efficiency. In non-isolated BDCs, interleaving is thus recommended where quick charging/discharging capability is required.

Furthermore, the controller mechanisms in any non-isolated BDC cannot give ZVS/ZCS naturally. Hence, soft-switching strategies must be considered to mitigate the switching losses. Excellent transient performance may be attained using the cascaded buck–boost architecture. It offers an option for improving the significant power transfer capability. An isolated BDC topology offers better internal safety over fault, which increases the system’s size, weight, and cost. A comparison between various converter topologies is listed in Table 1.

**Table 1.** Comparison between various converter topologies.

Ref. No	Converter Topology	Maximum Power	Number of Switches	Filter	Switching Mode	Switching Frequency (kHz)	Efficiency (%)	Applications
[12]	Auxiliary switching buck–boost converter	500 W	4	C	hard-switching	20	83	EV Auxillary Load Applications
[15]	Buck–boost converter	3.5 kW	2	LC	hard-switching	20	>90	Level 1 Charger, Light Duty EV Applications
[16]	Buck–boost	1.2 kW	2	LC	hard-switching	50	-	Level 1 Charger, Light Duty EV Applications
[17]	Dual full-bridge	3.3 kW	8	CLC	Soft switching	250	-	Level 1 Charger, Light Duty EV Applications
[18]	Interleaved buck–boost	30 kW	4	C	hard-switching	20	-	Level 2 Charger for Medium Power EV
[20]	Non-inverted buck–boost	18 kW	5	C	hard-switching	10	95.25	Level 2 Charger for Medium Power EV
[31]	Half-full-bridge resonant	10 kW	6	LC	Soft switching	90–150	>96 (G2V) >98 (V2G)	Level 2 Charger for Medium Power EV
[32]	Half-bridge resonant	3.3 kW	4	C	Soft switching	180–200	96	Level 1 Charger, Light Duty EV Applications
[36]	Dual full-bridge	250 W	8	C	Soft switching	100	93	EV Auxillary Load Applications
[37]	Full-bridge resonant	3.5 kW	8	C	Soft switching	85–145 (G2V), 40–110 (G2V), 200 at start-up	97.7 (G2V), 98.1 (V2G)	Level 1 Charger, Light Duty EV Applications
[38]	Dual voltage-fed	30 kW	8	C	hard-switching	20	-	Level 2 Charger for Medium Power EV
[42]	Half-full-bridge	1 kW	6	C	Soft switching	100	95.8	Level 1 Charger, Light Duty EV Applications

Table 1. Cont.

Ref. No	Converter Topology	Maximum Power	Number of Switches	Filter	Switching Mode	Switching Frequency (kHz)	Efficiency (%)	Applications
[43]	Cascaded buck–boost	9 kW	4	LC	hard-switching	20	91.61	Level 1 Charger, Light Duty EV Applications
[45]	Buck–boost (with auxiliary switching network)	500 W	2	LC	hard-switching	10	<85	EV Auxillary Load Applications
[46]	Interleaved buck–boost	400 W	4	C	hard-switching	20	>94	EV Auxillary Load Applications
[50]	Full-bridge resonant	6.6 kW	8	LC	Soft switching	50	97.7 (G2V), 97.3 (V2G)	Level 2 Charger for Medium Power EV
[51]	Full-bridge resonant	2.5 kW	10	C	Soft switching	50	96	Level 1 Charger, Light Duty EV Applications
[52]	Half-bridge resonant	3.3 kW	4	C	Soft switching	100–200	97.5 (G2V), 97.3 (V2G)	Level 1 Charger, Light Duty EV Applications
[53]	Half-bridge resonant	3.3 kW	4	LC	Soft switching	-	95.7 (G2V), 95.4 (V2G)	Level 1 Charger, Light Duty EV Applications

### 3. Conductive and Inductive Charger/Discharger

The use of the direct path for conductive charging and/or inductive discharging systems for power to flow between the utility grid and the electric vehicle battery [58–65]. EV owners can employ these systems to charge their cars rapidly. However, the owner of an electric vehicle (EV) must connect the cable every time needed to recharge or drain the electric vehicle battery [54]. The next method to transfer energy from the utility grid to the electric vehicle is to establish an inductive type network that uses resonance to send power over a wireless network medium. Nikola Tesla invented wireless-type inductive power transfer (IPT) in 1891. This idea was suggested for vehicle grid networks. This vehicle grid works with IPT. The system setup stays ideal, except that the vehicle and the grid need to install extra inductive charging and discharging circuitry.

An IPT system consists of a dual side, usually called pickup. It is isolated by [9] an air gap and magnetically associated with each other. It initiates at the pickup side to the average resonant frequency as it transfers to power at the primary side. The best part of Inductive power transfer is IPT, which makes life easier by removing contact wires and cords and isolating them from each other. Inductive systems also eliminate the chance of shock during wet conditions and wear and tear on the connector [66]. Conductive charging and inductive discharging systems can be neither built-in nor separate, and they might be placed ON or OFF condition of the EV inductive-type charging and discharging systems are usually non-integrated, which means that the pickup side is on an electric vehicle and not on the primary side.

Because of the worst magnetic coupling and greater flux leakage, these systems have a slow speed of charge and discharge, low power density, and poor efficiency, so they need higher supply voltage [9]. In inductive power transfer IPT-based vehicles to grid systems, current challenges such as reducing the amount of leakage flux and increasing the amount of power that can be transferred to the normal supply voltage and current rating [67]. In order to keep switching losses minimum, pulse width modulation technique control is not a good choice for IPT systems [9]. Conversely, the phase-modulated square pulses are utilized to regulate Inductive power transfer IPT systems to obtain both voltage  $v$  and current waveforms that look like sine waves. The control system is even more complicated by the availability of higher-frequency, higher-order resonance frequency systems because the resonant frequency depends on tolerances and temperature changes [11]. Moreover, in bidirectional type inductive power transfer IPT, the air gap needs two controlling techniques, one at the utility side and the other at the EV side, and these controllers have to be operated collaboratively [9]. However, the author [68] discusses only one controller on the grid side, which makes it possible for IPT to work both ways between the utility grid side and a single side of an electric vehicle EV.

Inductive charger/discharger systems also have a big problem between the primary and pickup side inductive platforms, which creates an imbalance. This, in turn, alters the magnetic coupling, which makes the change in resonant frequency and level of power transfer. Self-tuning control strategies in Inductive power transfer systems groove the converter operating frequency of the IPT systems at the resonant frequency, which removes the problem described in [69–75].

In [9], the authors suggested a current-sourced-based bidirectional converter interface that allows multiple EVs to be charged and discharged simultaneously through weak magnetic coupling with an efficiency of about 80%. Figure 19 shows the inductive power transfer of IPT-based vehicles to the grid V2G system that links in electric vehicles. Both the primary side and the pickup side are the same. They both have a full-bridge converter and an LCL resonant network connected in parallel. This makes the primary and pickup sides galvanically isolated. In order to connect more than one EV to the primary coil, each electric vehicle must have identical pickup coils, and the voltage in the primary side currently has to produce a standard path. When the LCL network on the pickup side of each one of the electric vehicles is synchronized to the path current frequency (20 kHz), the pickup side converters are run either in the inverting or rectifier mode, which depends on the direction

of the power flow. This creates a bidirectional power flow. The size and angle of the phase difference between the voltages on the primary and pickup sides determine the direction and amount of power flow. Power shifts from the pickup side to the primary side when there is a leading phase angle. Moreover, the power shift is taken from the primary to the pickup side when there is a trailing phase angle.

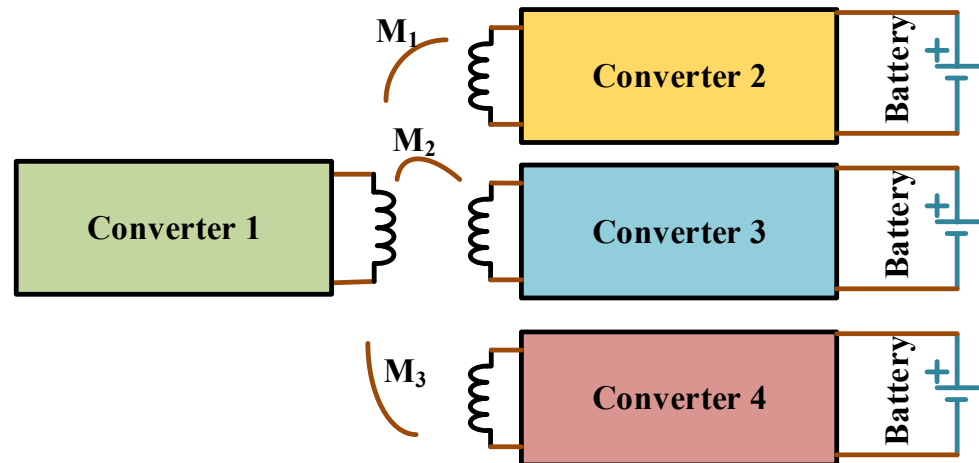


Figure 19. Multiple EVs charger.

The LCL network filters out all the high-order harmonics, both voltage and current, from the output side. On the primary or pickup side, a phase-modulated square-wave voltage is made by the same control systems comprising a triangular generator and a PI controller. The demerit of this mechanism is that the voltage at the primary side must be kept normal at all conditions to maintain a constant track current. It is impossible without properly using the control in the primary side voltage to change the pickup output power, but the only way to control this is to change the voltage on the pickup side. In the literature [76], there is an IPT based on V2G topology with a three-phase delta-connected magnetic field connected to a delta-connected three-phase pickup through an LCL-resonant type network.

A three-phase circuit and the pickup side can be coupled with a star configuration. This structure can quickly charge or discharge EVs because it uses weak magnetic coupling. This three-phase inductive power transfer IPT-based vehicle-to-grid system is superior to its single-phase counterpart because it uses fewer track currents to send the same quantity of power. The benefits include sending more power, being more efficient, and requiring a small filter.

In [11], the IPT-based V2G system utilizes two identical back-to-back converters, comprising of a utility grid side converter and a primary IPT, to convert energy into two stages. In the G2V mode, the primary side IPT modulates voltage level through DC-link into a resonance frequency of 20 kHz. The grid side converter works as a rectifier at the frequency of 50 Hz; resonance frequency (20 kHz) together into DC voltage to recharge the electrical device with the IPT pickup converter.

During V2G mode, the inductive power transfer and pickup converter converts the voltage of the EV battery into AC voltage at the resonance frequency. Moreover, the grid converter functions as an inverter for the primary power grid frequency, while the IPT converter converts the AC voltage level somewhere at the resonant frequency. Figure 20 shows the IPT system. Because of the tuned LCCL resonant system, which is operating using the current source, the high input inductor is no longer needed. This system is made up of  $L_1$ ,  $C_2$ , and  $C_1$  on the primary side of the converter and  $L_2$ ,  $C_3$ , and  $C_4$  on the pickup side of the converter. The inductance path of  $L_p$  is magnetically connected through the  $M$  to the pickup side coil  $L_1$ . This keeps the primary side and pickup sides from being electrically connected.

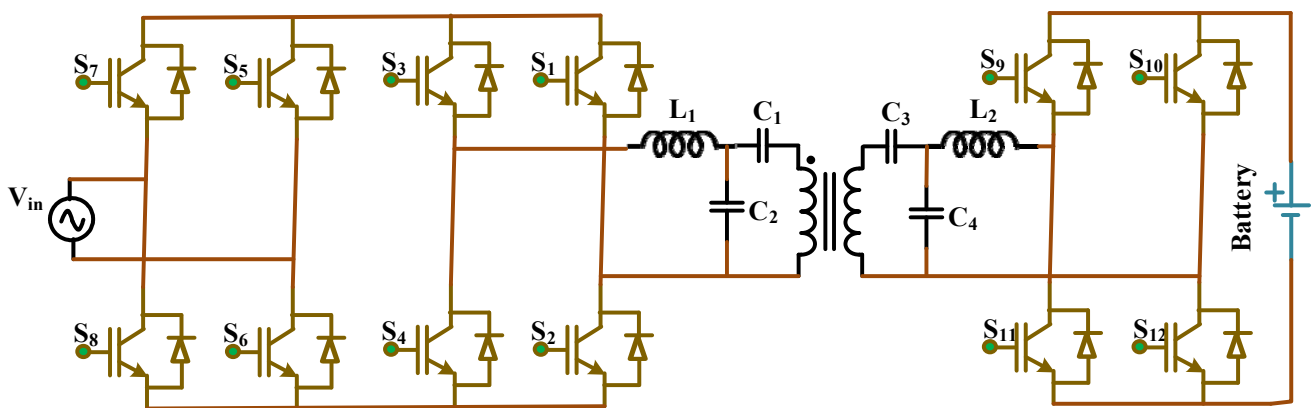


Figure 20. Bidirectional converters fed the IPT system.

The power flow direction is controlled by an open loop control system that accounts for the phase shifting at pickup side converters. It needs a high electrolytic capacitor and a high inductor at the input side to reduce low-frequency ripples in the DC link. This increases the overall cost and system size and makes it less reliable. For a 1.1 kW design, the system always gives an efficiency of 87%. The system loses most of its power because of its copper loss in the  $L_1$  and  $L_2$  inductors connected in series and the cables, and due to this reason, the average current value is higher, and the average value voltage is lower. The grid current has much harmonic distortion that is very difficult to fix, and it is also very difficult to achieve a unity power factor. The author in [11] suggested an inductive charging and discharging topology that uses the primary side of the back-to-back converter [11] on the grid side and a half-bridge [77] converter on the pickup side to obtain a power factor of 1 so that the current and voltage ripples on the DC link side are less.

The semi-bridge converter works at a PWM frequency. In this topology, a DC capacitor and pickup magnetic coupler are to be coupled in series to store or discharge energy to the load. In order to maintain the energy stored or discharged from the capacitor, the voltage across the semi-bridge is maintained constant by changing the duty cycle.

A bidirectional IPT-based charging and discharging system is described by using half-bridge architecture on the grid side converter and a voltage-fed supply half-bridge method on the battery side [78], as shown in Figure 21. The inductors  $L_1$  and  $L_2$  with the anti-parallel coupled switches  $S_1$  and  $S_3$  and  $S_2$  and  $S_4$  at every phase leg make up the current-fed supply at the half-bridge converter on the grid side. Here, one pair of switches is turned ON, and the other switches and diode will create a free-wheeling path for current. The grid side IPT has a series-parallel combination of resonant tanks composed of  $C_p$  and  $L_p$ . This tank reduces the maximum leakage from the coupling inductor and reduces the switching stress on the grid-side converter. On the other side of the battery is a resonant tank, i.e., LC made of  $L_s$  and  $C_s$ , which resonates no matter how much load is on it. Mutual inductance  $M$  links the primary as well as pickup sides together. In G2V mode, the converter at the battery side functions as a voltage-doubler circuit, while the other converter at the grid side performs as a high-frequency inverter. In V2G mode, the converter at the grid-side functions as a current doubler, while the battery side acts as a high-frequency inverter. The variable switching frequency, 40–60 kHz, is modulated to change the duty cycle, which regulates the power flow in either mode, which can aid the device in reaching ZVS. The full-load efficiency of the converter is above 90%.

In the IPT system, a matrix converter was utilized [79] on the primary side. The cost of the system can be reduced by changing AC frequency to HFAC at one stage and by connecting the matrix-based converter on the grid side and the primary side. The voltage level and direction can also be changed by adjusting the magnitude or relative phase angle of the primary side converter voltage and pickup side voltage. However, due to the lack of a freewheeling path and increased complexity in the robust design, the application-based systems become more complex. It was suggested in [69] that a matrix converter could

have a single phase that should be self-tuned, and the primary side is equipped with a matrix converter. The charging and discharging systems at the inductive grid side include an LC resonant tank and four bidirectional switches. The lack of an intermediary DC conversion stage and large capacitors at the DC bus means that it works at a resonant frequency of 35 kHz, is dependable, and has power density. The system employs the discrete-time sliding mode controlling [75] technique to manage the power flow and self-tune the converter switching frequency into the IPT system resonant frequency. The power electronic components are switched ON using the sliding mode control at resonant current zero-crossing positions. However, the converter experiences an irregular charging current at grid-side voltage zero-crossing places, which reduces the charging level. This erratic charging current may shorten the battery's working life. Based on the technique above, a three-phase matrix converter-based charging and discharging system was discussed in [70]. The converter is installed, and the central grid side converter employs six bidirectional switches, and each phase has two switches. The converter in dynamic IPT systems reaches ZCS by self-tuning and tracking the 35 kHz resonant frequency, assuring excellent efficiency of the inductive charging/discharging structure. The proposed converter exhibits the same drawback as that of the battery, and it requires an LC filter at the output side to remove unwanted ripples.

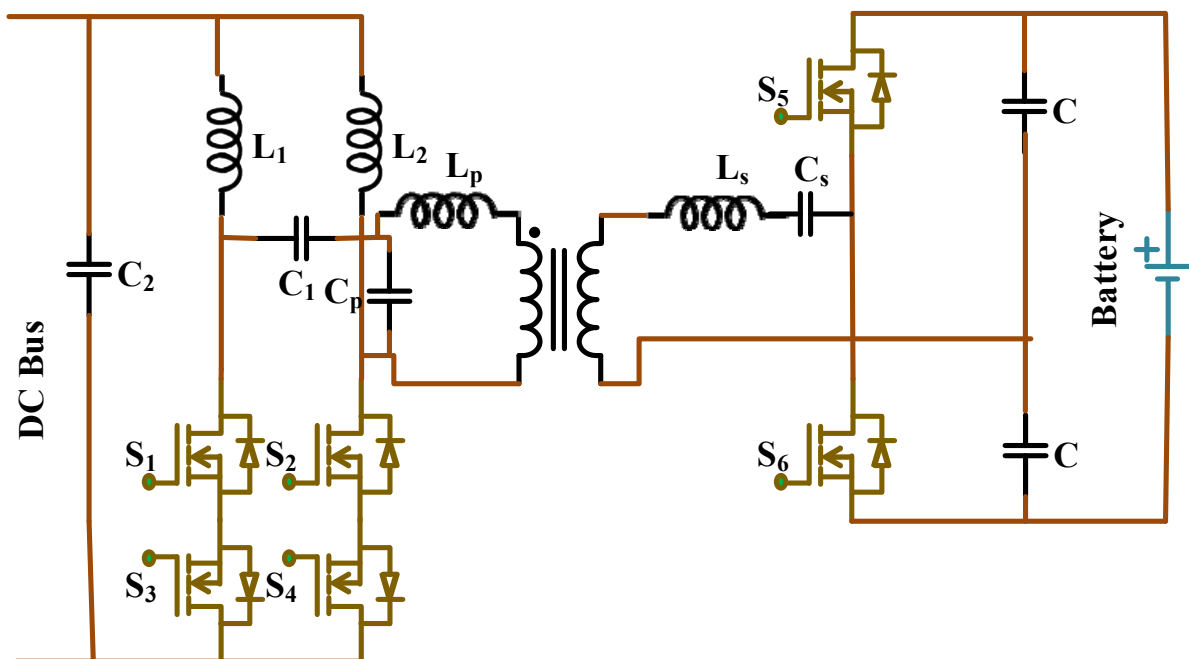


Figure 21. Current fed bidirectional converter topology.

In [74], it is suggested that an inductive charger/discharger system utilizes a single-phase matrix topology. However, the topology is the same as [69], and resonant frequency tracking is used to make this converter work consistently with the resonant current. It utilizes the quantum energy injection and regeneration concept to regulate how much energy can be stored in the resonant tank and how much energy flows between grid-to-vehicle and vehicle-to-grid modes. In this case, the resonant tank receives energy from the grid, which is tuned to match the half cycles of the resonant current.

To make sure that devices switch smoothly, they are operated at the points where the resonant current crosses zero. The converter's efficiency is more than 90% for high power transfer, which can be a positive indication. Ref. [80] discusses the bidirectional IPT structure, which could hold a huge air gap of 12–20 cm. The system is made up of two identical full-bridge BADCs on the primary sides and pickup sides, which are detached by a high-frequency transformer. These converters work at expected frequencies composed

of self-inductance and resonating capacitance. For a maximum load of 6.4 kW, the power transfer efficiency lies between 88.1% and 95.3% for an air gap of 12 to 20 cm. Bac et al. glanced into a G2V power flow IPT system with a SiC-based matrix converter methodology. The converter has a surprisingly low efficiency of 85% when the gap of the coil is as small as 12 cm and delivers 300 W of power in the G2V mode [81].

#### 4. Comparison of Different Charging/Discharging Systems

The different kinds of charging and discharging systems for vehicle-to-grid are discussed in the above sections. In order to obtain the ideal system for vehicle-to-grid applications, it is essential to compare these systems. The difference between the different types of charging lots is shown in Table 2; for charger/discharger systems, it can be hard to establish the specific condition for making the analysis among all the available systems. A few of these criteria have been proposed, and Table 3 compares the different systems based on these criteria. It should be emphasized that there is significant conductive overlap. Such systems have been eliminated from the discussion and non-integrated structures with other classes.

**Table 2.** Cohesive operation of different types of charger and dischargers lots.

		Discharging					
		On-board	Off-board	Integrated	Non-integrated	Conductive	Inductive
Charging	On-board	Yes	No	Yes	Yes	Yes	-
	Off-board	No	Yes	No	Yes	Yes	-
	Integrated	Yes	No	Yes	No	Yes	No
	Non-integrated	Yes	Yes	No	Yes	Yes	Yes
	Conductive	Yes	Yes	Yes	Yes	Yes	No
	Inductive	-	-	No	Yes	No	Yes

**Table 3.** Comparison based on different types of charging and discharging systems.

	Cost, Weight, and Volume	Infrastructure	Capacity of Charging and Discharging	Efficiency of Charging and Discharging	Practical Challenges
On-board and non-integrated	Huge	Less	Medium	Huge	Less cost, weight, and volume
Off-board	Less	Huge	Huge	Huge	More risk
Integrated	Less	Less	Huge	Medium	Generation of flux can be produced
Inductive	Huge	Huge	Less	Less	Less capability of power transfer

When the various systems are compared using the suggested criteria, it becomes clear that integrated charger/discharger systems now represent the most affordable option for V2G applications. The issue of electromagnetic flux creation, though used in the V2G and G2V modes, results in an idle driving torque electric vehicle, which must be appropriately responded to. System reconfiguration has been used to address these issues by employing multi-phase motors with auxiliary switches, which makes the system more expensive and complex. Only if the challenges posed by their poorer efficiency and power transfer performance are overcome will inductive systems compete with their conductive counterparts in V2G applications.

Furthermore, it is essential to carefully position the primary and pickup coils to increase the power transmission rate, raising doubts about the practicality of inductive

charging/discharging system arrangements. Systems with off-board can be designed to enable quick charging and discharging of electric vehicles because they are less constrained by size than on-board systems. However, to implement V2G via off-board devices, the government organization or utility grid must construct the supplied equipment throughout all of the cities and towns in a given state or country, which would necessitate a substantial investment. Due to this, since most electric vehicles are plug-in hybrid electric vehicles (PHEVs) with medium-sized batteries, for the on-board, it appears that a non-integrated charging and discharging system is, due to its ease, the ideal choice for V2G applications. It offers versatility and a respectable charging and discharging speed. The current study aims to increase the ability to lower the cost of achieving S.A.E. Level-3 compliance for on-board systems Size and price.

### 5. Energy Management in EV

This section discusses the features of the proposed electric vehicle charging and discharging scheduling algorithm, together with the energy management scheme of the microgrid. It is presumed that each electric vehicle has access to a bidirectional EV charger coupled with a PV-based charging station and may either charge or discharge its battery. The two-way electric vehicle charger allows the user to control the connected EV's ability to switch between discharging and charging operations. Depending on the fluctuating patterns of the local load profile and PV power output, the maximum amount of electricity that can be discharged from parked electric vehicles is made available. According to the EV's data, any parked electric vehicle becomes a potential participant in a charging or discharging process. Then, depending upon the EV charging/discharging candidates, a "charging", "discharging", or "idle" action is given to the transfer function of each parked EV using the multi-objective process. The switching feature of each electric vehicle is applied to the multi-objective optimization in order to simultaneously take into account the operating cost of PV-based charging stations, PV power usage, grid reliance, utilization of EVs, current state of charge (SOC) values of EVs, and the residual parking time of EVs. Figure 22 demonstrates the flowchart of (V2G and G2V, RES and no EV) to obtain the estimated result of various successful EV outcomes while integrating 10 EVs. This is performed in order to gain knowledge of how each EV will interact with one another.

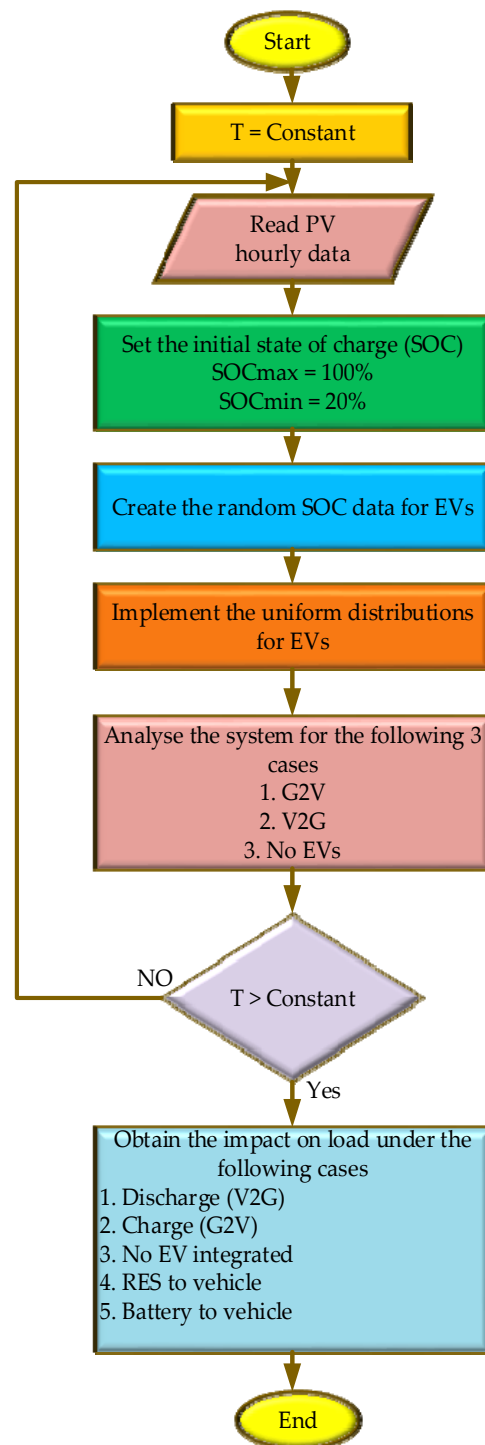


**Figure 22.** Flowchart of (V2G and G2V, RES and no EV) to obtain the estimation result of various successful EV outcomes.

## 6. Recent Trends

Integrating V2G networks into electricity grids is a difficult task in charging stations. According to the V2G theory, electric vehicle owners have to charge their cars at off-peak times and discharge them at high peaks to assist the grid utility function. However, this charging and discharging assumption is frequently disregarded by EV owners, leading to an erratic pattern of EV charging and discharging in a V2G system. This results in instability in voltage, power restrictions, disturbances in harmonics, distribution losses in the low-voltage grid, and a shorter operational life span of cables and distribution

transformers [82]. When compared to V2G, the issue is worse in G2V mode. Employing renewable resources such as solar systems and wind energy in an intelligent grid-based future architecture can relieve the issues above [82–110].

Grid-tied energy storage devices are usually necessary for intermittent renewable-fed electric grids to provide a steady power supply. The concept behind connecting vehicle-to-grid systems with renewable sources-fed grids is to temporarily store fluctuating electricity produced during off-peak hours by renewable sources in the batteries of numerous connected electric vehicles. This reduces or eliminates the requirement for expensive grid-coupled energy storage devices and aids in boosting the electric vehicle without affecting the grid's operation. Through V2G, the grid is fed with the battery capacity of numerous linked electric vehicles during peak hours to make up for any energy shortages. As a result, the grid's stability, dependability, and efficiency are restored [82]. The grid is employed to provide power to charge linked electric vehicles. The power supplied from renewable energy sources is insufficient to satisfy those demands.

The grid-side energy demand will be significantly decreased because renewable energy can be produced locally. Refs. [83–85] offer a comprehensive analysis of the effects of connecting V2G networks and renewable energy sources. Solar photovoltaic (PV) is one of the most recommended nonconventional sources for its integration into charging and discharging systems. Refs. [86,87] examined a variety of system topologies for electric vehicles and photovoltaic hybrid charging and discharging. For connecting photovoltaic arrays and electric vehicles to the AC grid through a common bus, multiport converters are typically used in integrated renewable sources-based charging and discharging stations [88–90].

This system allows for connecting numerous PV arrays and EVs using a single independent multiport converter. A significant high-power BADC supplied by numerous multiport transforms the DC bus voltage. Converters convert from grid voltage to AC power. If the case common bus is AC, the isolated multiport converter can contain the BADC for connecting the utility grid, increasing the system's control flexibility and fault tolerance. The requirement of one BADC increases the cost of the system under this architecture for each multiport converter. It has also been suggested that multiplexing EV chargers and dischargers could lower the infrastructure for charging and discharging systems. A single EV charger/discharger is used to charge/discharge several long-parked EVs [91].

PV array power is in the form of DC, and the voltage obtained is less than the DC-bus voltage. Therefore, a UDC must be used to boost the DC voltage because it cannot be used directly to charge the EV battery. Additionally, PV converters use MPPT [92] algorithms to regulate the sporadic power produced by PV arrays to match the constant DC voltage. Because of its high gain in voltage and a low number of components, non-isolated boost UDC with maximum power point tracking provides the most recommended PV converter methodology [86,93,94]. In [95], a three-phase interleaved boost UDC with MPPT based on SiC was studied to implement in PV converters. In [93], a boost UDC and a Z source network are employed to exhibit improved voltage gain. Here, the BDC is eliminated by directly connecting the EV battery to a three-phase full-bridge BADC on one side and the PV converter on the other.

The charging/discharging system in [96] was evaluated using a quasi-Z-source network, which showed an increasingly wider range of input–output voltage at a greater price and larger size. Authors in [89,94,97,98] and in [86,89,91,93,97–99] suggested a non-isolated buck–boost BDC and single-phase or three-phase full-bridge BADC, both used in integrated renewable EV charging/discharging systems. The charging and discharging system suggested in [94] was recommended to use a four-legged unidirectional voltage inverter topology. Its major function is to change the DC voltage output of the PV converter. The major drawback is that the usage of two inverters increases the cost of the system. In [97,98], the systems for high power transfer employ a buck–boost-based BDC with two interleaved phases that are not isolated.

The safety reasons for HF isolation between the utility grid and the electric vehicle is desirable [86]. However, the non-isolated buck–boost converter mentioned falls under this criterion. According to standards [100], isolation between linked EVs is desirable when connecting numerous EVs. As a result, researchers also investigated transformers with multi-winding, which has only one winding on one side but more windings on the other side. Care should be taken while designing the transformer and the complex controller. However, standards are not required for isolating between the AC or DC bus and the photovoltaic system. The bi-directional power flow is discussed in [88].

A three-phase transformer with one winding on one side charges or discharges a battery bank by the six-legged structure of BADC. The other side of the transformer has two windings that connect the AC network through a three-phase matrix converter and an electric vehicle battery through a three-full-bridge-based BADC to make a multiport converter, which was proposed in [101]. This high-power multiport converter can connect through V2G without incorporating renewable energy systems. Additionally, the network is quite expensive due to the heavy use of switching devices.

A three-port SiC-based high power-density charging/discharging system connecting photovoltaic, EVs, and the grid, was suggested in [90]. There has been the use of a three-phase interleaved boost structure for a three-phase full-bridge architecture has been utilized in the PV boost converter. It is employed for the grid-tied BADC, whereas the EV-side BDC has a single interleaved four-stage flyback topology. In [99], the author described the structure where a grid and EV are connected through a quasi-Z-source boost converter. The charging/discharging system incorporates a double-winding HF isolated transformer, where each PV converter's winding is linked to a half-bridge on the PV side of the BDC.

An integrated charger and discharger used for on-board charging stations were studied by Hsu et al., in addition to the AC grid using an off-board boost converter [102]. The vehicle on-board non-isolated buck–boost based BDC, which has the capability of regenerative braking and feeds the permanent magnet DC motor. The interconnected charger/discharger system uses a full-bridge BADC, and the motor windings are used as energy storage inductors that were added externally as grid interfacing to enable the power flows from G2V and V2G [105].

Due to geographical limitations, wind energy conversion systems (WECS) and electric vehicle combinations have not received as much research as photovoltaic solar arrays [103]. Common parts of a WECS include a turbine, a generator, a converter, and a maximum power point controller. WECS-integrated smart grids that facilitate V2G have been the subject of some literature studies [92,104,105]. The wind-powered system for discharging and charging described in [92] employs a leading, high-power, three-phase full-bridge BADC and 15 separate DAB BDCs. to enable the continuous charging/discharging of 15 EVs.

Solar and wind-powered hybrid charging and discharging systems that work with EVs have been documented in [106,107]. A hybrid PHEV [108] with a photovoltaic array and a small wind power turbine is suggested in place of the internal combustion engine. The PHEV allows G2V and V2G, which makes the weight of the electric vehicle. IPT for integration of renewable charging and discharging systems, which offer the essential separation between the EV and the grid and numerous linked electric vehicles, have also been examined. These works use converters on the primary and pickup sides comparable to those suggested in [9].

Currently, research is concentrated on innovative electric vehicle charging and discharging, which is anticipated to impact the creation of global energy regulations substantially. The EV can be continuously charged and discharged from a renewable energy source, and the integrated grid is emphasized by the notion that charging and discharging allow the power consumption to be monitored and regulated in line with the requirements of the grid [83,109,110]. In this case, estimates for optimization methods and renewable energy will be used to determine how closely EV charging patterns should mimic low-cost energy sources, including renewable power generation and off-peak hours [84,91,104].

This idea will also minimize the grid impact of large-scale EVs charging and discharging simultaneously. It will help additional renewable sources obtain adoption by offering a significant amount of energy storage for erratic renewable energy.

Additionally, V2G enables the assurance of other services such as frequency control, compensation of reactive power, the possibility of load balancing, peak load shaving, voltage control, active power management, and reactive power adjustment [7,104]. It will enhance the performance and functioning of the smart grid integration in the future for renewable energy. The global energy economy will change due to the lower cost of EV charging of the integrated EV and renewable energy smart grid in the future [104].

## 7. Inferences from the Review

The electronic switches include silicon carbide and gallium nitride. They have properties such as high breakdown voltage, band gap, saturation velocity, and thermal conductivity, which result in huge power handling capacity but are smaller in size and produce fewer losses, which are of both unidirectional and bidirectional conducting nature. GaN devices are used for low-power applications (<600 V) and provide excellent switching performance. For the eight-switch topology, the BADC is operated as an active rectifier when operated during G2V mode and as a regulated source during V2G mode, which can contribute to maintaining the power factor of the grid. Two different modes of operation could be set as inverter and rectifier under motoring mode and regenerative mode, respectively. The structure can improve reliability by decreasing the THD level. Thus, the system can produce an efficiency of not less than 97% in both modes of operation when choosing a wide range of voltage, even though the applications of BADC suffer from more conduction loss. In three-level topology, the BADC functions as an active rectifier when it is set to the G2V mode. When operating in the V2G mode, BADC operates as a regulated source of current that contributes power to the utility grid for maintaining the power factor.

In single-stage topology, variable dependent load frequency is maintained with the frequency ranges from 20 kHz to 120 kHz, but the frequency level is maintained less during low load conditions. However, the half-bridge topology is replaced by the full-bridge topology on the input side, leading to increased power devices. Topology based on a matrix converter is typically for power frequency to AC grid voltage conversion into high-frequency AC grid voltage; it requires the AC voltage to DC voltage and DC to AC conversion stages, and more extensive and pricier capacitors are required. However, these large and costly components are eliminated by matrix converters.

In isolated topologies, galvanic isolation, the flexibility of control, the soft-switching capability of soft-switching, less stress in voltage, higher efficiency, high capability of power, density, symmetrical, expandable design, enhanced bidirectional type DC-DC converters (BDCs), and a capacity of power flow are some of the key benefits of the DAB architecture. Because of the absence of the high-frequency isolation transformer, the benefits of non-isolated methodology are fewer switches and passive components, lesser costs, and a minimum footprint than isolated methodology. For non-isolated type topologies, it has been reported that a FB type of bidirectional converter linked with a non-isolated buck-boost converter can regulate both real power and reactive powers. In resonant topologies, researchers are investigating substantially larger attention to resonant-type DC-DC converters for a large range of voltage applications. As they do not require clamp or snubber circuitry, they provide incredibly high operation on high frequency, outstanding efficiency, minimal electromagnetic interference, and lesser components. Additionally, the bidirectional DC-DC converter has a sluggish overvoltage response.

## 8. Conclusions

A thriving technology called vehicle-to-grid (V2G) enables EVs to function as distributed resources that may store or release energy whenever required, enabling a bidirectional power transfer between the grid and the EV. This increases the overall capacity for power generation while simultaneously improving the grid stability, dependability, and

efficiency. Bi-directional electronic converters are commonly incorporated to enable the power flow between G2V and V2G. These converters have been successfully developed and applied in V2G systems. This work examined the different BADC and BDC topologies used in any V2G systems. Additionally, a comparative investigation is made and determined the best architecture for V2G applications. For the V2G applications, different charger/discharger system designs, including on-board and off-board, integrated and non-integrated, and conductive and inductive, were examined.

According to the review, a typical V2G connection bidirectional charging and discharging mechanism should conform to the following: (a) prompt response to a momentary requirement of load; (b) manipulation of the grid and EV; (c) efficient high power transfer; (d) high density for fast charging; (e) reducing losses due to switching, device stress, and EMI by simple power switching; (f) fewer components and high-frequency operation to reduce size and price; (g) a straightforward and effective control excellent reliability for widespread deployment and system; (h) correction of the power factor grid's stability and low harmonic distortion; and (i) must meet the standards and specifications for connectivity.

In contrast to modern EVs that use huge batteries, the majority of bidirectional converters created for V2G connections have a rated power below 10 kW, which is noticeably low. One of the critical reasons for this low power rating is a restriction of power. Of course, one way to raise the converter power rating is to connect power devices in parallel, which increases the system cost and footprint. SiC and GaN are the two wide bandgap semiconductors that have opened up new possibilities for developing highly efficient bidirectional converters that can quickly discharge or charge EV batteries. The recent research on intelligent EV charging and discharging can also improve the functionality and performance of the planned framework for an intelligent grid integrated with renewable energy sources.

**Author Contributions:** Conceptualization, S.P. and P.V.; methodology, N.R.; software, M.B.; validation, S.P., N.R. and P.V.; formal analysis, V.B., L.P. and S.M.; investigation, M.B.; resources, L.P.; data curation, V.B.; writing—original draft preparation, S.P., P.V. and N.R.; writing—review and editing, S.P., P.V. and N.R.; visualization, M.B., V.B., L.P. and S.M.; supervision, V.B.; project administration, L.P.; funding acquisition, V.B., L.P., S.M. All authors have read and agreed to the published version of the manuscript.

**Funding:** This paper was supported by the following projects: TN02000025 “National Centre for Energy II”, and project CK04000060 “Developing analytical tools for an effective transition to electromobility” and Government of India, Department of Science and Technology (DST) Science and Engineering Research Board (SERB) Core Research Grant C.R.G./2020/004073.

**Data Availability Statement:** Not applicable.

**Acknowledgments:** Not applicable.

**Conflicts of Interest:** The authors declare no conflict of interest.

## Nomenclature

V2G	Vehicle–grid
EV	Electric vehicle
G2V	Grid–vehicle
DC	Direct current
AC	Alternate current
ICE	Internal composition engine
PHEV	Plug-in hybrid electric vehicle
IC	Internal composition
RES	Renewable energy sources
THD	Total harmonic distortion
PV	Photo voltaic

SiC	Silicon carbide
BADC	Bidirectional AC-DC Converter
V2H	vehicle-home
FB	Full bridge
PRC	Proportional resonant controller
PSO	Particle swarm optimization
FOC	Field-oriented control
PFC	Power factor correction
ZVS	Zero-voltage switching
SPWM	Sinusoidal pulse width modulation
PWM	Pulse width modulation
PLL	Phase-locked loop
VA	Voltage ampere
EMI	Electromagnetic interference
DAB	Dual active bridge
BDC	Bidirectional DC-DC converters
ZCS	Zero current switching
HV	High voltage
LV	Low voltage
MOSFET	Metal oxide semiconductor field effect transistor
IPT	Inductive power transfer

## References

1. Kempton, W.; Tomić, J. Vehicle-to-grid power implementation: From stabilizing the grid to supporting large-scale renewable energy. *J. Power Sources* **2005**, *144*, 280–294. [[CrossRef](#)]
2. Global EV Outlook. International Energy Agency (IEA). 2017. Available online: <https://www.iea.org/publications/freepublications/publication/GlobalEVOutlook2017> (accessed on 15 December 2022).
3. Kempton, W.; Letendre, S.E. Electric vehicles as a new power source for electric utilities. *Transp. Res. Part D Transp. Environ.* **1997**, *2*, 157–175. [[CrossRef](#)]
4. Kempton, W.; Tomic, J.; Letendre, S.; Brooks, A.; Lipman, T. *Vehicle-to-Grid Power: Battery, Hybrid and Fuel Cell Vehicles as Resources for Distributed Electric Power in California*; Report # IUCD-ITS-RR 01-03; Institute of Transportation Studies: Davis, CA, USA, 2005.
5. Tomić, J.; Kempton, W. Using fleets of electric-drive vehicles for grid support. *J. Power Sources* **2007**, *168*, 459–468. [[CrossRef](#)]
6. Shanmugam, Y.; Vishnuram, P.; Savio, D.; Bajaj, M.; Yadav, A.; Nauman, D.; Khurshaid, T.; Kamel, S. Solar-Powered Five-Leg Inverter-Driven Quasi-Dynamic Charging for A Slow-Moving Vehicle. *Front. Energy Res.* **2023**, *11*, 185. [[CrossRef](#)]
7. Rahman, M.; Rafi, F.; Hossain, M.; Lo, J. Power control and monitoring of smart grid with EVs. In *Vehicle-to-Grid: Linking Electric Vehicles to the Smart Grid*; Lu, J., Hossain, J., Eds.; Asia Pacific, IET Press: Stevenage, UK, 2015; pp. 107–155.
8. Kempton, W.; Tomić, J. Vehicle-to-grid power fundamentals: Calculating capacity and net revenue. *J. Power Sources* **2005**, *144*, 268–279. [[CrossRef](#)]
9. Madawala, U.K.; Thrimawithana, D.J. A Bidirectional Inductive Power Interface for Electric Vehicles in V2G Systems. *IEEE Trans. Ind. Electron.* **2011**, *58*, 4789–4796. [[CrossRef](#)]
10. Castillo-Calzadilla, T.; Cuesta, M.; Quesada, C.; Olivares-Rodriguez, C.; Macarulla, A.; Legarda, J.; Borges, C. Is a massive deployment of renewable-based low voltage direct current microgrids feasible? Converters, protections, controllers, and social approach. *Energy Rep.* **2022**, *8*, 12302–12326. [[CrossRef](#)]
11. Weearsinghe, S.; Thrimawithana, D.J.; Madawala, U.K. Modeling Bidirectional Contactless Grid Interfaces with a Soft DC-Link. *IEEE Trans. Power Electron.* **2014**, *30*, 3528–3541. [[CrossRef](#)]
12. Han, H.; Liu, Y.; Sun, Y.; Wang, H.; Su, M. A Single-Phase Current-Source Bidirectional Converter for V2G Applications. *J. Power Electron.* **2014**, *14*, 458–467. [[CrossRef](#)]
13. Rahulkumar, J.; Narayanamoorthi, R.; Vishnuram, P.; Bajaj, M.; Blazek, V.; Prokop, L.; Misak, S. An Empirical Survey on Wireless Inductive Power Pad and Resonant Magnetic Field Coupling for In-Motion EV Charging System. *IEEE Access* **2023**, *11*, 4660–4693. [[CrossRef](#)]
14. Pinto, J.G.; Monteiro, V.; Goncalves, H.; Exposto, B.; Pedrosa, D.; Couto, C.; Afonso, J.L. Bidirectional battery charger with Grid-to-Vehicle, Vehicle-to-Grid and Vehicle-to-Home technologies. In Proceedings of the IECON 2013—39th Annual Conference of the IEEE Industrial Electronics Society, Vienna, Austria, 10–13 November 2013; pp. 5934–5939. [[CrossRef](#)]
15. Pinto, J.G.; Monteiro, V.; Gonçalves, H.; Afonso, J.L. On-board reconfigurable battery charger for electric vehicles with traction-to-auxiliary mode. *IEEE Trans. Veh. Technol.* **2014**, *63*, 1104–1116. [[CrossRef](#)]
16. Verma, A.K.; Singh, B.; Shahani, D. Grid to vehicle and vehicle to grid energy transfer using single-phase bidirectional AC-DC converter and bidirectional DC-DC converter. In Proceedings of the 2011 International Conference on Energy, Automation and Signal, Bhubaneswar, India, 28–30 December 2011; pp. 1–5. [[CrossRef](#)]

17. Pahlevani, M.; Jain, P. A Fast DC-Bus Voltage Controller for Bidirectional Single-Phase AC/DC Converters. *IEEE Trans. Power Electron.* **2015**, *30*, 4536–4547. [[CrossRef](#)]
18. Hegazy, O.; Van Mierlo, J.; Lataire, P. Control and Analysis of an Integrated Bidirectional DC/AC and DC/DC Converters for Plug-In Hybrid Electric Vehicle Applications. *J. Power Electron.* **2011**, *11*, 408–417. [[CrossRef](#)]
19. Erb, D.C.; Onar, O.C.; Khaligh, A. An integrated bi-directional power electronic converter with multi-level AC-DC/DC-AC converter and non-inverted buck-boost converter for PHEVs with minimal grid level disruptions. In Proceedings of the 2010 IEEE Vehicle Power and Propulsion Conference, Lille, France, 1–3 September 2010; pp. 1–6. [[CrossRef](#)]
20. Onar, O.C.; Kobayashi, J.; Erb, D.C.; Khaligh, A. A Bidirectional High-Power-Quality Grid Interface with a Novel Bidirectional Noninverted Buck–Boost Converter for PHEVs. *IEEE Trans. Veh. Technol.* **2012**, *61*, 2018–2032. [[CrossRef](#)]
21. Zhu, L.; Wu, H.; Mu, T.; Yang, F.; Ma, X. An asymmetrical three-level dual-input bidirectional DC/AC converter with improved conversion efficiency for vehicle-to-grid application. In Proceedings of the 2017 IEEE Applied Power Electronics Conference and Exposition (APEC), Tampa, FL, USA, 26–30 March 2017; pp. 2062–2067. [[CrossRef](#)]
22. Jauch, F.; Biela, J. Single-phase single-stage bidirectional isolated ZVS AC-DC converter with PFC. In Proceedings of the 2012 15th International Power Electronics and Motion Control Conference (EPE/PEMC), Novi Sad, Serbia, 4–6 September 2012; pp. LS5d.1-1–LS5d.1-8. [[CrossRef](#)]
23. Vaishnav, S.N.; Krishnaswami, H. Single-stage isolated bi-directional converter topology using high frequency AC link for charging and V2G applications of PHEV. In Proceedings of the 2011 IEEE Vehicle Power and Propulsion Conference, Chicago, IL, USA, 6–9 September 2011; pp. 1–4. [[CrossRef](#)]
24. Pal, A.; Basu, K. A bidirectional snubber less soft-switched high frequency link DC/AC converter. In Proceedings of the 2016 7th India International Conference on Power Electronics (IICPE), Patiala, India, 17–19 November 2016; pp. 1–8. [[CrossRef](#)]
25. Su, M.; Wang, H.; Sun, Y.; Yang, J.; Xiong, W.; Liu, Y. AC/DC Matrix Converter with an Optimized Modulation Strategy for V2G Applications. *IEEE Trans. Power Electron.* **2013**, *28*, 5736–5745. [[CrossRef](#)]
26. Sandoval, J.J.; Essakiappan, S.; Enjeti, P. A bidirectional series resonant matrix converter topology for electric vehicle DC fast charging. In Proceedings of the 2015 IEEE Applied Power Electronics Conference and Exposition (APEC), Charlotte, NC, USA, 15–19 March 2015; pp. 3109–3116. [[CrossRef](#)]
27. Varajão, D.; Araújo, R.E.; Miranda, L.M.; Lopes, J.P.; Weise, N.D. Control of an isolated single-phase bidirectional AC-DC matrix converter for V2G applications. *Electr. Power Syst. Res.* **2017**, *149*, 19–29. [[CrossRef](#)]
28. Thrimawithana, D.J.; Madawala, U.K.; Twiname, R.; Vilathgamuwa, D.M. A novel matrix converter based resonant dual active bridge for V2G applications. In Proceedings of the 2012 10th International Power & Energy Conference (IPEC), Ho Chi Minh City, Vietnam, 12–14 December 2012; pp. 503–508. [[CrossRef](#)]
29. Choi, W.; Han, D.; Morris, C.T.; Sarlioglu, B. Achieving high efficiency using SiC MOSFETs and reduced output filter for grid-connected V2G inverter. In Proceedings of the IECON 2015—41st Annual Conference of the IEEE Industrial Electronics Society, Yokohama, Japan, 9–12 November 2015; pp. 003052–003057. [[CrossRef](#)]
30. Xue, L.; Shen, Z.; Boroyevich, D.; Mattavelli, P.; Diaz, D. Dual Active Bridge-Based Battery Charger for Plug-in Hybrid Electric Vehicle with Charging Current Containing Low Frequency Ripple. *IEEE Trans. Power Electron.* **2015**, *30*, 7299–7307. [[CrossRef](#)]
31. Wang, X.; Jiang, C.; Lei, B.; Teng, H.; Bai, H.K.; Kirtley, J.L. Power-Loss Analysis and Efficiency Maximization of a Silicon-Carbide MOSFET-Based Three-Phase 10-kW Bidirectional EV Charger Using Variable-DC-Bus Control. *IEEE J. Emerg. Sel. Top. Power Electron.* **2016**, *4*, 880–892. [[CrossRef](#)]
32. Tang, Y.; Lu, J.; Wu, B.; Zou, S.; Ding, W.; Khaligh, A. An Integrated Dual-Output Isolated Converter for Plug-in Electric Vehicles. *IEEE Trans. Veh. Technol.* **2018**, *67*, 966–976. [[CrossRef](#)]
33. Jain, M. Bi-Directional DC-DC Converter for Low Power Applications. Master’s Thesis, Department of Electrical and Computer Engineering, Concordia University, Montreal, QC, Canada, 1998.
34. Zhao, B.; Song, Q.; Liu, W.; Sun, Y. Overview of Dual-Active-Bridge Isolated Bidirectional DC–DC Converter for High-Frequency-Link Power-Conversion System. *IEEE Trans. Power Electron.* **2014**, *29*, 4091–4106. [[CrossRef](#)]
35. Du, Y.; Lukic, S.; Jacobson, B.; Huang, A. Review of high power isolated bi-directional DC-DC converters for PHEV/EV DC charging infrastructure. In Proceedings of the 2011 IEEE Energy Conversion Congress and Exposition, Phoenix, AZ, USA, 17–22 September 2011; pp. 553–560.
36. Xuewei, P.; Rathore, A.K. Novel Bidirectional Snubberless Naturally Commutated Soft-Switching Current-Fed Full-Bridge Isolated DC/DC Converter for Fuel Cell Vehicles. *IEEE Trans. Ind. Electron.* **2014**, *61*, 2307–2315. [[CrossRef](#)]
37. Zahid, Z.U.; Dalala, Z.M.; Chen, R.; Chen, B.; Lai, J.-S. Design of Bidirectional DC–DC Resonant Converter for Vehicle-to-Grid (V2G) Applications. *IEEE Trans. Transp. Electrification.* **2015**, *1*, 232–244. [[CrossRef](#)]
38. Xu, B.; Wang, H.; Sun, H.; Wang, Y. Design of a bidirectional power converter for charging pile based on V2G. In Proceedings of the 2017 IEEE International Conference on Industrial Technology (ICIT), Toronto, ON, Canada, 22–25 March 2017; pp. 527–531. [[CrossRef](#)]
39. Olivares-Rodríguez, C.; Castillo-Calzadilla, T.; Kamara-Esteban, O. Bio-inspired Approximation to MPPT Under Real Irradiation Conditions. In *Intelligent Distributed Computing XII*; Springer: Cham, Switzerland, 2018; Volume 798, pp. 107–118. [[CrossRef](#)]
40. Shanmugam, Y.; Narayanamoorthi, R.; Vishnuram, P.; Bajaj, M.; AboRas, K.M.; Thakur, P.; Kitmo, A. Systematic Review of Dynamic Wireless Charging System for Electric Transportation. *IEEE Access* **2022**, *10*, 133617–133642. [[CrossRef](#)]

41. Shi, Y.; Li, R.; Xue, Y.; Li, H. Optimized Operation of Current-Fed Dual Active Bridge DC–DC Converter for PV Applications. *IEEE Trans. Ind. Electron.* **2015**, *62*, 6986–6995. [[CrossRef](#)]
42. Rathore, A.; Prasanna, U. Analysis, design, and experimental results of novel snubberless bidirectional naturally clamped ZCS/ZVS current fed half-bridge DC/DC converter for fuel cell vehicles. *IEEE Trans. Ind. Electron.* **2013**, *60*, 4482–4491. [[CrossRef](#)]
43. Khan, M.A.; Husain, I.; Sozer, Y. A Bidirectional DC–DC Converter with Overlapping Input and Output Voltage Ranges and Vehicle to Grid Energy Transfer Capability. *IEEE J. Emerg. Sel. Top. Power Electron.* **2014**, *2*, 507–516. [[CrossRef](#)]
44. Restrepo, M.; Morris, J.; Kazerani, M.; Canizares, C.A. Modeling and Testing of a Bidirectional Smart Charger for Distribution System EV Integration. *IEEE Trans. Smart Grid* **2018**, *9*, 152–162. [[CrossRef](#)]
45. Sun, Y.; Liu, W.; Su, M.; Li, X.; Wang, H.; Yang, J. A unified modeling and control of a multi-functional current source-typed converter for V2G application. *Electr. Power Syst. Res.* **2014**, *106*, 12–20. [[CrossRef](#)]
46. Peng, T.; Yang, P.; Dan, H.; Wang, H.; Han, H.; Yang, J.; Wang, H.; Dong, H.; Wheeler, P. A Single-Phase Bidirectional AC/DC Converter for V2G Applications. *Energies* **2017**, *10*, 881. [[CrossRef](#)]
47. Yang, P.; Peng, T.; Wang, H.; Han, H.; Yang, J.; Wang, H. A single-phase current source bidirectional converter for V2G application. In Proceedings of the 2017 IEEE 3rd International Future Energy Electronics Conference and ECCE Asia (IFEEC 2017–ECCE Asia), Kaohsiung, Taiwan, 3–7 June 2017; pp. 704–709.
48. Kang, T.; Kim, C.; Suh, Y.; Park, H.; Kang, B.; Kim, D. A design and control of bi-directional non-isolated DC-DC converter for rapid electric vehicle charging system. In Proceedings of the 2012 Twenty-Seventh Annual IEEE Applied Power Electronics Conference and Exposition (APEC), Orlando, FL, USA, 5–9 February 2012; pp. 14–21. [[CrossRef](#)]
49. Ibanez, F.M.; Echeverria, J.M.; Vadillo, J.; Fontan, L. A Step-Up Bidirectional Series Resonant DC/DC Converter Using a Continuous Current Mode. *IEEE Trans. Power Electron.* **2015**, *30*, 1393–1402. [[CrossRef](#)]
50. Lee, B.-K.; Kim, J.-P.; Kim, S.-G.; Lee, J.-Y. An Isolated/Bidirectional PWM Resonant Converter for V2G(H) EV On-Board Charger. *IEEE Trans. Veh. Technol.* **2017**, *66*, 7741–7750. [[CrossRef](#)]
51. Twiname, R.P.; Thrimawithana, D.J.; Madawala, U.K.; Baguley, C.A. A New Resonant Bidirectional DC–DC Converter Topology. *IEEE Trans. Power Electron.* **2014**, *29*, 4733–4740. [[CrossRef](#)]
52. Zou, S.; Lu, J.; Mallik, A.; Khaligh, A. Bi-Directional CLLC Converter with Synchronous Rectification for Plug-In Electric Vehicles. *IEEE Trans. Ind. Appl.* **2018**, *54*, 998–1005. [[CrossRef](#)]
53. Kwon, M.; Choi, S. An Electrolytic Capacitorless Bidirectional EV Charger for V2G and V2H Applications. *IEEE Trans. Power Electron.* **2017**, *32*, 6792–6799. [[CrossRef](#)]
54. Yilmaz, M.; Krein, P.T. Review of Battery Charger Topologies, Charging Power Levels, and Infrastructure for Plug-In Electric and Hybrid Vehicles. *IEEE Trans. Power Electron.* **2013**, *28*, 2151–2169. [[CrossRef](#)]
55. Haghbin, S.; Lundmark, S.; Alakula, M.; Carlson, O. Grid-Connected Integrated Battery Chargers in Vehicle Applications: Review and New Solution. *IEEE Trans. Ind. Electron.* **2013**, *60*, 459–473. [[CrossRef](#)]
56. Khan, M.A.; Husain, I.; Sozer, Y. Integrated Electric Motor Drive and Power Electronics for Bidirectional Power Flow Between the Electric Vehicle and DC or AC Grid. *IEEE Trans. Power Electron.* **2013**, *28*, 5774–5783. [[CrossRef](#)]
57. Zhang, F.; Wang, X.; Liao, Q.; Auth, C.G. Highly integrated bidirectional vehicle-to-grid (V2G) for electric vehicles based on open winding permanent magnet synchronous motor. In Proceedings of the 2017 20th International Conference on Electrical Machines and Systems (ICEMS), Sydney, NSW, Australia, 11–14 August 2017; pp. 1–4. [[CrossRef](#)]
58. Leonori, S.; Baldini, L.; Rizzi, A.; Mascioli, F.M.F. A Physically Inspired Equivalent Neural Network Circuit Model for SoC Estimation of Electrochemical Cells. *Energies* **2021**, *14*, 7386. [[CrossRef](#)]
59. Pa, L.; Zhang, C. An integrated multifunctional bidirectional AC/DC and DC/DC converter for electric vehicles applications. *Energies* **2016**, *9*, 493.
60. Subotic, I.; Bodo, N.; Levi, E.; Jones, M. On-board integrated battery charger for EVs using an asymmetrical nine-phase machine. *IEEE Trans. Ind. Electron.* **2015**, *62*, 3285–3295. [[CrossRef](#)]
61. Castillo-Calzadilla, T.; Alonso-Vicario, A.; Borges, C.E.; Martin, C. E-Mobility in Positive Energy Districts. *Buildings* **2022**, *12*, 264. [[CrossRef](#)]
62. Hu, K.-W.; Yi, P.-H.; Liaw, C.-M. An EV SRM Drive Powered by Battery/Supercapacitor with G2V and V2H/V2G Capabilities. *IEEE Trans. Ind. Electron.* **2015**, *62*, 4714–4727. [[CrossRef](#)]
63. Ebrahimi, S.; Taghavi, M.; Tahami, F.; Oraee, H.; Tagliavi, M. A single-phase integrated bidirectional plug-in hybrid electric vehicle battery charger. In Proceedings of the IECON 2014—40th Annual Conference of the IEEE Industrial Electronics Society, Dallas, TX, USA, 29 October–1 November 2014; pp. 1137–1142. [[CrossRef](#)]
64. Ebrahimi, S.; Taghavi, M.; Tahami, F.; Oraee, H. Integrated bidirectional isolated soft-switched battery charger for vehicle-to-grid technology using 4-Switch 3 $\Phi$ -rectifier. In Proceedings of the IECON 2013—39th Annual Conference of the IEEE Industrial Electronics Society, Vienna, Austria, 10–13 November 2013; pp. 906–911.
65. Ebrahimi, S.; Akbari, R.; Tahami, F.; Oraee, H. An Isolated Bidirectional Integrated Plug-in Hybrid Electric Vehicle Battery Charger with Resonant Converters. *Electr. Power Compon. Syst.* **2016**, *44*, 1371–1383. [[CrossRef](#)]
66. Miskiewicz, R.; Moradewicz, A. Contact-less power interface for plug-in electric vehicles in V2G systems. *Bull. Pol. Acad. Sci. Tech. Sci.* **2011**, *59*, 561–568.

67. Miller, J.M.; Daga, A. Elements of Wireless Power Transfer Essential to High Power Charging of Heavy Duty Vehicles. *IEEE Trans. Transp. Electrification*. **2015**, *1*, 26–39. [[CrossRef](#)]
68. Madawala, U.; Thrimawithana, D. New technique for inductive power transfer using a single controller. *IET Power Electron.* **2012**, *5*, 248–256. [[CrossRef](#)]
69. Vishnuram, P.; Alagarsamy, S.; Krishnasamy, V.; Bajaj, M.; Khurshaid, T.; Nauman, D.; Kamel, S. A comprehensive review on EV power converter topologies charger types infrastructure and communication techniques. *Front. Energy Res.* **2023**, *11*, 1103093. [[CrossRef](#)]
70. Moghaddami, M.; Sarwat, A. A Three-Phase AC-AC Matrix Converter with Simplified Bidirectional Power Control for Inductive Power Transfer Systems. In Proceedings of the 2018 IEEE Transportation Electrification Conference and Expo (ITEC), Long Beach, CA, USA, 13–15 June 2018; pp. 380–384. [[CrossRef](#)]
71. Moghaddami, M.; Sundararajan, A.; Sarwat, A.I. A self-tuning variable frequency control for multi-level contactless Electric Vehicle charger. In Proceedings of the 2016 IEEE International Conference on Power Electronics, Drives and Energy Systems (PEDES), Trivandrum, India, 14–17 December 2016; pp. 1–5. [[CrossRef](#)]
72. Moghaddami, M.; Sarwat, A. Self-Tuning Variable Frequency Controller for Inductive Electric Vehicle Charging with Multiple Power Levels. *IEEE Trans. Transp. Electrification*. **2018**, *3*, 488–495. [[CrossRef](#)]
73. Moghaddami, M.; Sundararajan, A.; Sarwat, A.I. A Power-Frequency Controller with Resonance Frequency Tracking Capability for Inductive Power Transfer Systems. *IEEE Trans. Ind. Appl.* **2017**, *54*, 1773–1783. [[CrossRef](#)]
74. Moghaddami, M.; Sarwat, A.I. Single-Phase Soft-Switched AC-AC Matrix Converter with Power Controller for Bidirectional Inductive Power Transfer Systems. *IEEE Trans. Ind. Appl.* **2018**, *54*, 3760–3770. [[CrossRef](#)]
75. Van Der Pijl, F.F.A.; Castilla, M.; Bauer, P. Adaptive Sliding-Mode Control for a Multiple-User Inductive Power Transfer System without Need for Communication. *IEEE Trans. Ind. Electron.* **2013**, *60*, 271–279. [[CrossRef](#)]
76. Thrimawithana, D.J.; Madawala, U.K. A three-phase bi-directional IPT system for contactless charging of electric vehicles. In Proceedings of the IEEE International Symposium on Industrial Electronics, Gdansk, Poland, 27–30 June 2011; pp. 1957–1962. [[CrossRef](#)]
77. Shanmugam, Y.; Sathik, J.; Almakhles, D.J. A Comprehensive Review of the On-Road Wireless Charging System for E-Mobility Applications. *Front. Energy Res.* **2022**, *10*, 926270. [[CrossRef](#)]
78. Samanta, S.; Rathore, A.K.; Thrimawithana, D.J. Bidirectional Current-Fed Half-Bridge (C) (LC)–(LC) Configuration for Inductive Wireless Power Transfer System. *IEEE Trans. Ind. Appl.* **2017**, *53*, 4053–4062. [[CrossRef](#)]
79. Thrimawithana, D.J.; Madawala, U.K. A novel matrix converter based bi-directional IPT power interface for V2G applications. In Proceedings of the 2010 IEEE International Energy Conference, Manama, Bahrain, 18–22 December 2010; pp. 495–500. [[CrossRef](#)]
80. Lee, J.Y.; Han, B. A bidirectional wireless power transfer EV charger using self resonant P.W.M. *IEEE Trans. Power Electron.* **2015**, *30*, 1784–1787. [[CrossRef](#)]
81. Bac, N.X.; Vilathgamuwa, D.; Madawala, U. A SiC-based matrix converter topology for inductive power transfer system. *IEEE Trans. Power Electron.* **2014**, *29*, 4029–4038. [[CrossRef](#)]
82. Vishnuram, P.; Nastasi, B. Wireless Chargers for Electric Vehicle: A Systematic Review on Converter Topologies, Environmental Assessment, and Review Policy. *Energies* **2023**, *16*, 1731. [[CrossRef](#)]
83. Yuvaraja, S.; Narayanamoorthi, R. A Five Leg Converter with Multi-Transmitter for an In-Motion Charging System. *J. Phys. Conf. Ser.* **2022**, *2335*, 012054. [[CrossRef](#)]
84. Mouli, G.R.C.; Bauer, P. Optimal System Design for a Solar Powered EV Charging Station. In Proceedings of the 2018 IEEE Transportation Electrification Conference and Expo (ITEC), Long Beach, CA, USA, 13–15 June 2018; pp. 1094–1099.
85. Mwasilu, F.; Justo, J.J.; Kim, E.-K.; Do, T.D.; Jung, J.-W. Electric vehicles and smart grid interaction: A review on vehicle to grid and renewable energy sources integration. *Renew. Sustain. Energy Rev.* **2014**, *34*, 501–516. [[CrossRef](#)]
86. Mouli, G.R.C.; Bauer, P.; Zeman, M. Comparison of system architecture and converter topology for a solar powered electric vehicle charging station. In Proceedings of the 2015 9th International Conference on Power Electronics and ECCE Asia (ICPE-ECCE Asia), Seoul, Republic of Korea, 1–5 June 2015; pp. 1908–1915. [[CrossRef](#)]
87. Pathipati, V.; Shafiei, A.; Carli, G.; Williamson, S. Integration of renewable energy sources into the transportation and electricity sectors. In *Technologies and Applications for Smart Charging of Electric and Plug-in Hybrid Vehicles*; Veneri, O., Ed.; Springer: Cham, Switzerland, 2017; pp. 65–110.
88. Krishnaswami, H.; Mohan, N. Three-port series-resonant DC-DC converter to interface renewable energy sources with bidirectional load and energy storage ports. *IEEE Trans. Power Electron.* **2009**, *24*, 2289–2297. [[CrossRef](#)]
89. Monteiro, V.; Pinto, J.G.; Afonso, J.L. Experimental Validation of a Three-Port Integrated Topology to Interface Electric Vehicles and Renewables with the Electrical Grid. *IEEE Trans. Ind. Inform.* **2018**, *14*, 2364–2374. [[CrossRef](#)]
90. Mouli, G.R.C.; Schijffelen, J.; Heuvel, M.V.D.; Kardolus, M.; Bauer, P. A 10 kW Solar-Powered Bidirectional EV Charger Compatible with Chademo and COMBO. *IEEE Trans. Power Electron.* **2018**, *34*, 1082–1098. [[CrossRef](#)]
91. Mouli, G.R.C.; Kefayati, M.; Baldick, R.; Bauer, P. Integrated PV Charging of EV Fleet Based on Energy Prices, V2G, and Offer of Reserves. *IEEE Trans. Smart Grid* **2017**, *10*, 1313–1325. [[CrossRef](#)]
92. Fathabadi, H. Novel wind powered electric vehicle charging station with vehicle-to-grid (V2G) connection capability. *Energy Convers. Manag.* **2017**, *136*, 229–239. [[CrossRef](#)]

93. Leonori, S.; Rizzoni, G.; Mascioli, F.M.F.; Rizzi, A. Intelligent energy flow management of a nanogrid fast charging station equipped with second life batteries. *Int. J. Electr. Power Energy Syst.* **2020**, *127*, 106602. [[CrossRef](#)]
94. Verma, A.K.; Singh, B.; Shahani, D.T.; Jain, C. Grid-interfaced Solar Photovoltaic Smart Building with Bidirectional Power Flow Between Grid and Electric Vehicle with Improved Power Quality. *Electr. Power Compon. Syst.* **2016**, *44*, 480–494. [[CrossRef](#)]
95. Mouli, G.R.C.; Schijffelen, J.H.; Bauer, P.; Zeman, M. Design and Comparison of a 10-kW Interleaved Boost Converter for PV Application Using Si and SiC Devices. *IEEE J. Emerg. Sel. Top. Power Electron.* **2017**, *5*, 610–623. [[CrossRef](#)]
96. Venkatesan, M.; Rajamanickam, N.; Vishnuram, P.; Bajaj, M.; Blazek, V.; Prokop, L.; Misak, S. A Review of Compensation Topologies and Control Techniques of Bidirectional Wireless Power Transfer Systems for Electric Vehicle Applications. *Energies* **2022**, *15*, 7816. [[CrossRef](#)]
97. Choe, G.-Y.; Kim, J.-S.; Lee, B.-K.; Won, C.-Y.; Lee, T.-W. A Bi-directional battery charger for electric vehicles using photovoltaic PCS systems. In Proceedings of the 2010 IEEE Vehicle Power and Propulsion Conference, Lille, France, 1–3 September 2010; pp. 1–6. [[CrossRef](#)]
98. Kim, N.-H.; Cheo, G.-Y.; Lee, B.-K. Design and Control of an Optimized Battery Charger for an xEV Based on Photovoltaic Power Systems. *J. Electr. Eng. Technol.* **2014**, *9*, 1602–1613. [[CrossRef](#)]
99. Singh, S.; Carli, G.; Azeez, N.; Williamson, S. Modeling, design, control, and implementation of a modified Z-Source in-tergrated PV/Grid/EV DC Charger/Inverter. *IEEE Trans. Ind. Electron.* **2018**, *65*, 5213–5220. [[CrossRef](#)]
100. SAE Standard J1772; SAE Electric Vehicle and Plug-in Hybrid Electric Vehicle Conductive Charge Coupler. SAE International: Warrendale, PA, USA, 2010.
101. Waltrich, G.; Duarte, J.L.; Hendrix, M.A.M. Multiport converter for fast charging of electrical vehicle battery: Focus on DC/AC converter. In Proceedings of the IECON 2011—37th Annual Conference of the IEEE Industrial Electronics Society, Melbourne, VIC, Australia, 7–10 November 2011; pp. 3626–3633. [[CrossRef](#)]
102. Hsu, Y.-C.; Kao, S.-C.; Ho, C.-Y.; Jhou, P.-H.; Lu, M.-Z.; Liaw, C.-M. On an Electric Scooter with G2V/V2H/V2G and Energy Harvesting Functions. *IEEE Trans. Power Electron.* **2018**, *33*, 6910–6925. [[CrossRef](#)]
103. Bhatti, A.R.; Salam, Z.; Aziz, M.J.A.; Yee, K.P.; Ashique, R. Electric vehicles charging using photovoltaic: Status and technological review. *Renew. Sustain. Energy Rev.* **2016**, *54*, 34–47. [[CrossRef](#)]
104. Sharma, A.; Sharma, S. Review of power electronics in vehicle-to-grid systems. *J. Energy Storage* **2019**, *21*, 337–361. [[CrossRef](#)]
105. Miller, J.M.; Onar, O.C.; Chinthavali, M. Primary-Side Power Flow Control of Wireless Power Transfer for Electric Vehicle Charging. *IEEE J. Emerg. Sel. Top. Power Electron.* **2015**, *3*, 147–162. [[CrossRef](#)]
106. Qiu, C.; Chau, K.; Liu, C.; Chan, C. Overview of wireless power transfer for electric vehicle charging. In Proceedings of the 2013 World Electric Vehicle Symposium and Exhibition (EVS27), Barcelona, Spain, 17–20 November 2013; pp. 1–9. [[CrossRef](#)]
107. Choi, S.Y.; Gu, B.W.; Jeong, S.Y.; Rim, C.T. Advances in Wireless Power Transfer Systems for Roadway-Powered Electric Vehicles. *IEEE J. Emerg. Sel. Top. Power Electron.* **2015**, *3*, 18–36. [[CrossRef](#)]
108. Li, S.; Liu, Z.; Zhao, H.; Zhu, L.; Shuai, C.; Chen, Z. Wireless Power Transfer by Electric Field Resonance and Its Application in Dynamic Charging. *IEEE Trans. Ind. Electron.* **2016**, *63*, 6602–6612. [[CrossRef](#)]
109. Budhia, M.; Covic, G.; Boys, J. A new IPT magnetic coupler for electric vehicle charging systems. In Proceedings of the IECON 2010—36th Annual Conference on IEEE Industrial Electronics Society, Glendale, AZ, USA, 7–10 November 2010; pp. 2487–2492.
110. Nagendra, G.R.; Covic, G.A.; Boys, J.T. Determining the physical size of inductive couplers for IPT EV systems. In Proceedings of the Conference Proceedings-IEEE Applied Power Electronics Conference and Exposition-APEC, Fort Worth, TX, USA, 16–20 March 2014; pp. 3443–3450.

**Disclaimer/Publisher’s Note:** The statements, opinions and data contained in all publications are solely those of the individual author(s) and contributor(s) and not of MDPI and/or the editor(s). MDPI and/or the editor(s) disclaim responsibility for any injury to people or property resulting from any ideas, methods, instructions or products referred to in the content.